Inorg. Chem. **2008**, *47*, 3772−3786

New Extended Magnetic Systems Based on Oxalate and Iron(III) Ions

Donatella Armentano,[†] Teresa F. Mastropietro,[†] Giovanni De Munno,[*,†] Patrizia Rossi,[‡] Francesc Lloret,[§] and Miguel Julve[§]

Dipartimento di Chimica, Università della Calabria, via P. Bucci 14/c, 87036 Rende, Cosenza, Italy, Dipartimento di Energetica, Università di Firenze, via Santa Marta 3, 50134 Firenze, Italy, and Departament de Química Inorgànica/Instituto de Ciencia Molecular, Universitat de Valencia, Polígono La Coma s/n, 46980 Paterna (València), Spain

Received December 12, 2007

A series of oxalate-bridged iron(III) complexes have been synthesized by the reaction of $FeCl_3$ with oxalic acid (H_2ox) and XCl, where X is a substituted univalent ammonium or an alkaline cation. We have obtained basically two different types of compounds by varying the nature and the shape of the counterion, with the dimensionality of the resulting product being strongly influenced by the counterion. Three-dimensional (3D) networks of oxo- and oxalato-bridged iron(III) ions of the general formula $\{X_2[Fe_2O(ox)_2Cl_2]\cdot pH_2O\}_n$ have been obtained for X = Li^+ (**1**), Na^+ (**2**), and K^+ (**3**) with $p = 4$ and X = $MeNH_3^+$ (**4**), $Me_2NH_2^+$ (**5**), and $EtNH_3^+$ (**6**) with $p = 2$. Similar 3D hydroxo- and oxalato-bridged iron(III) networks of the formula $\{X[Fe_2(OH)(ox)_2Cl_2]\cdot 2H_2O\}_n$ resulted for X = $EtNH_3^+$ (**7a**) and $PrNH_3^+$ (**8**). Compound **7a** undergoes a solid-to-solid transformation, leading to a new species of the formula $\{(H_3O)(EtNH_3)[Fe_2O(ox)_2Cl_2]\cdot H_2O\}_n$ (**7b**). Chainlike compounds of the formula $\{X_2[Fe_2(ox)_2Cl_4]\cdot pH_2O\}_n$ [X = $Me_2NH_2^+$(**9**, $p = 1$), Me_3NH^+ (**10**, $p = 2$), and Me_4N^+ (**11**, $p = 0$)] have been obtained for the bulkier alkylammonium cations. Magnetic susceptibility measurements in the temperature range 1.9–295 K show the occurrence of weak ferromagnetic ordering due to spin canting in the 3D networks **1**−**8**, with the value of the critical temperature (T_c) varying with the cation in the range 26 K (**2**) to 70 K (**8**) without significant structural modifications. The last three one-dimensional compounds exhibit the typical behavior of antiferromagnetically coupled chains of interacting spin sextets [$J = -8.3$ (**9**), -6.9 (**10**), and -8.4 (**11**) cm^{-1} with $H = -J\sum_i S_i S_{i+1}$].

Introduction

In recent years, the design and synthesis of metal−organic framework (MOF) have attracted considerable attention in supramolecular chemistry and crystal engineering,[1,2] mainly because of the fact that these supramolecular assemblies have interesting structures as well as potentially useful properties such as magnetic,[3] catalytic,[4] and nonlinear optical activity or electrical conductivity.[5–8] The use of mononuclear coordination complexes as architectural units to build supramolecular arrays is a developing strategy in this field that has the appealing possibility of constructing porous materials.[9]

* To whom correspondence should be addressed. E-mail: demunno@unical.it. Phone: (+39) 0984 492068. Fax: (+39) 0984 493309.
† Università della Calabria.
‡ Università di Firenze.
§ Universitat de Valencia.

(1) (a) Choi, H. J.; Suh, M. P. *J. Am. Chem. Soc.* **1998**, *120*, 10622. (b) Cheetham, A. K.; Ferey, G.; Loiseau, T. *Angew. Chem., Int. Ed.* **1999**, *38*, 3268. (c) Long, D. L.; Blake, A. J.; Champness, N. R.; Schröder, M. *Chem. Commun.* **2000**, 1369. (d) James, S. L. *Chem. Soc. Rev.* **2003**, *32*, 276.
(2) (a) Janiak, C. *Dalton Trans.* **2003**, 2781. (b) Day, P. In *Supramolecular Engineering of Synthetic Metallic Materials*; Veciana, J., Rovira, C., Amabilino, D. B., Eds.; NATO ASI Series C518; Kluwer: Dordrecht, The Netherlands, 1999; p 253.
(3) Seo, J. S.; Whang, D. M.; Lee, H.-Y.; Jun, S. I.; Oh, J.-H.; Jeon, Y. J.; Kim, K. *Nature* **2000**, *404*, 982.
(4) *Molecule Based Materials*; Miller, J. S., Drillon, M., Eds.; Wiley-VCH: Weinheim, Germany, 2001.
(5) (a) Coronado, E.; Galán-Mascarós, J. R.; Gómez-García, C. J.; Laukhin, V. *Nature* **2000**, *408*, 447. (b) Coronado, E.; Palomares, E. *J. Mater. Chem.* **2005**, *35*(36), 3593.
(6) Karasawa, S.; Sano, Y.; Akita, T.; Koga, N.; Itoh, T.; Iwamura, H.; Rabu, P.; Drillon, M. *J. Am. Chem. Soc.* **1998**, *120*, 10080.
(7) Yaghi, O. M.; Li, H.; Davis, C.; Richardson, D.; Groy, T. L. *Acc. Chem. Res.* **1998**, *31*, 474.
(8) Lacroix, P. G.; Malfant, I.; Benard, S.; Yu, P.; Riviere, E.; Nakatani, K. *Chem. Mater.* **2001**, *13*, 441.
(9) (a) Eddaoudi, M.; Moler, D. B.; Li, H. L.; Reineke, T. M.; O'Keeffe, M.; Yaghi, O. M. *Acc. Chem. Res.* **2001**, *34*, 319. (b) Chae, H. K.; Kim, J.; Friedrichs, O. D.; O'Keefe, M.; Yaghi, O. M. *Angew. Chem., Int. Ed.* **2003**, *42*, 3907.

10.1021/ic702403h CCC: $40.75
Published on Web 03/22/2008

A careful selection of the metal ions, peripheral ligands, and modular bridging groups is required in order to produce defined architectures with interesting functions in a controlled fashion.[10]

In the search for new molecule-based magnets during the past decade, oxalato-bridged heteropolynuclear complexes have played an important role in the development of chemistry of molecular solids with interesting physical, electrical, magnetic, and optical properties.[5,11–13] In fact, the oxalate has appeared to be a suitable candidate for this because of its ability to mediate strong magnetic interactions between the paramagnetic centers that it links when adopting the bisbidentate coordination mode.[2,12a,14,15] One of the most remarkable features of molecule-based materials is the way that the magnetic properties may be tuned through subtle variations in the molecular chemistry.[12a,14,15] A striking example of this general statement is the elegant and diverse series of anionic two-[16–23] and three-dimensional (*n*D)[24–30] oxalato-bridged bimetallic networks whose dimensionality is governed by the nature of the templating cation. Some of them exhibit ferro-[16] ferri-,[31] or antiferromagnetic[20,29,30] long-range ordering with values of the critical temperature (T_c) ranging from 5 up to 48 K. The synthetic strategy consists of polymerization of the trisoxalate $[M(ox)_3]^{(6-m)-}$ mononuclear precursor into two or three directions, with the formation of the 2D or 3D motif being dependent on the choice of the template counterion. The 2D magnetic materials are obtained by reacting the trisoxalate salts with both divalent and trivalent transition-metal ions in the presence of a wide range of organic cations, mainly tetraalkylammonium and tetraarylphosphonium/arsonium.[16,23] The common formula is $C^+M^{II}M'^{III}(ox)_3$ (C^+ = organic cation), with the M^{II} and M'^{III} metal ions alternating in an honeycomb lattice and being bridged by the bisbidentate oxalate. The magnetic properties for such systems have been found to be strongly sensitive to small chemical variations of C^+.[18,20] Finally, helical 3D networks are associated with the use of $[M(bpy)_3]^{m+}$ (bpy = 2,2′-bipyridine) as the templating cation.[24–30]

Some years ago and in the context of our current research work concerning the reactivity of trivalent first-row transition-metal ions toward the oxalate ligand, we prepared and characterized the first example of a 3D oxalate- and oxo-bridged iron(III) complex of the formula $\{(NH_4)_2[Fe_2O(ox)_2Cl_2]\cdot 2H_2O\}_n$ that exhibits magnetic ordering due to spin canting with a T_c value of ca. 40 K.[32] More recently, in an attempt to explore the influence of the cation on the structure and magnetic properties of this type of network, we carried out a preliminary investigation of the compounds of the formula $\{X_2[Fe_2O(ox)_2Cl_2]\cdot 2H_2O\}_n$ [X = $MeNH_3^+$ (**4**), $Me_2NH_2^+$ (**5**), and $EtNH_3^+$ (**6**)][33] and $\{X[Fe_2(OH)(ox)_2Cl_2]\cdot 2H_2O\}$ [X = $EtNH_3^+$ (**7a**) and $PrNH_3^+$ (**8**)].[34] They are all 3D materials that exhibit magnetic ordering with values of T_c ranging from 40 to 70 K depending on the nature of counterion. We also noticed that the use of bulkier cations such as Me_3NH^+ and Me_4N^+ afforded oxalato-bridged iron(III) chains.[33] With these features in mind, we carried out a systematic study of the reaction of $FeCl_3$ with oxalic acid (H_2ox) and XCl, where X^+ is a substituted univalent ammonium or an alkaline cation, and all of the obtained results are presented here. They concern the preparation, crystal structure, and magnetic properties of the 3D complexes $\{X_2[Fe_2O(ox)_2Cl_2]\cdot pH_2O\}$ [X = Li^+ (**1**), Na^+ (**2**), and K^+ (**3**) with $p = 4$ and X = $MeNH_3^+$ (**4**), $Me_2NH_2^+$ (**5**), and $EtNH_3^+$ (**6**) with $p = 2$], $\{X[Fe_2(OH)(ox)_2Cl_2]\cdot 2H_2O\}_n$ [X = $EtNH_3^+$ (**7a**) and $PrNH_3^+$ (**8**)] and $\{(H_3O)(EtNH_3)[Fe_2O(ox)_2Cl_2]\cdot H_2O\}_n$ (**7b**) as well as the chain compounds

(10) (a) De Cola, L.; Belser, P. *Coord. Chem. Rev.* **1998**, *177*, 301. (b) Rao, C. N. R.; Natarajan, S.; Vaidhyanathan, R. *Angew. Chem., Int. Ed.* **2004**, *43*, 1466. (c) Imai, H.; Inoue, K.; Kikuchi, K.; Yoshida, Y.; Ito, M.; Sunahara, T.; Onaka, S. *Angew. Chem., Int. Ed.* **2004**, *43*, 5618.

(11) (a) For example, see: Zhong, Z. J.; Matsumoto, N.; Okawa, H.; Kida, S. *Chem. Lett.* **1990**, 87. (b) Chen, N. Y.; Keading, W. W.; Dwyer, F. G. *J. Am. Chem. Soc.* **1997**, *101*, 6783. (c) Pilkington, M.; Decurtins, S. In *Magnetism: Molecules to Materials II*; Miller, J. S., Drillon, M., Eds.; VCH: Weinheim, Germany, 2001; p 339.

(12) (a) Miller, J. S. *Adv. Mater.* **2002**, *14*, 1105. and references cited therein. (b) Andrés, R.; Brissard, M.; Gruselle, M.; Train, C.; Vaissermann, J.; Malézieux, B.; Jamet, J.-P.; Verdaguer, M. *Inorg. Chem.* **2001**, *40*, 4633. (c) Coronado, E.; Curreli, S.; Giménez-Saiz, C.; Gómez-García, C. J. *J. Mater. Chem.* **2005**, *14*, 1429.

(13) Pilkington, M.; Decurtins, S. *Comprehensive Coordination Chemistry II. From Biology to Nanotechnology*; McCleverty J. A., Meyer, T. J., Eds.; Elsevier: Amsterdam, The Netherlands, 2004; Vol. *7*, p 177. and references cited therein.

(14) (a) Kahn, O. *Molecular Magnetism*; VCH: New York, 1993. (b) Miller, J. S. *Adv. Mater.* **2002**, *14*, 1105.

(15) Decurtins, S.; Pellaux, R.; Hauser, A.; Von Arx, M. E. In *Magnetism: A Supramolecular Function*; Kahn, O., Ed.; NATO-ASI Series C484; Kluwer Academic Press: New York, 1996; p 487.

(16) Tamaki, H.; Zhong, Z. J.; Matsumoto, N.; Kida, S.; Koikawa, M.; Achiwa, N.; Hashimoto, Y.; Okawa, H. *J. Am. Chem. Soc.* **1992**, *114*, 6974.

(17) Atovmyan, L. O.; Shilov, G. V.; Lyubovskaya, R. N.; Zhilyaeva, E. I.; Ovanesyan, N. S.; Pirumova, S. I.; Gusakovskaya, I. G. *JETP Lett.* **1993**, *58*, 766.

(18) Decurtins, S.; Schmalle, H. W.; Oswald, H. R.; Linden, A.; Ensling, J.; Gütlich, P.; Hauser, A. *Inorg. Chim. Acta* **1994**, *216*, 65.

(19) Reiff, W. M.; Kreisz, J.; Meda, L.; Kirss, R. U. *Mol. Cryst. Liq. Cryst.* **1995**, *273*, 181.

(20) Mathonière, C.; Nuttall, C. J.; Carling, S. G.; Day, P. *Inorg. Chem.* **1996**, *35*, 1201.

(21) Carling, S. G.; Mathonière, C.; Day, P.; Abdul Malik, K. M.; Coles, S. J.; Hursthouse, M. B. *J. Chem. Soc., Dalton Trans.* **1996**, 1839.

(22) Pellaux, R.; Schmalle, H. W.; Huber, R.; Fischer, P.; Hauss, T.; Ouladdiaf, B.; Decurtins, S. *Inorg. Chem.* **1997**, *36*, 2301.

(23) Coronado, E.; Galán-Mascarós, J. R.; Martí-Gastaldo, C. *J. Mater. Chem.* **2006**, *26*, 2685.

(24) Decurtins, S.; Schmalle, H. W.; Schneuwly, P.; Oswald, H. R. *Inorg. Chem.* **1993**, *32*, 1888.

(25) Decurtins, S.; Schmalle, H. W.; Schneuwly, P.; Ensling, J.; Gütlich, P. *J. Am. Chem. Soc.* **1994**, *116*, 9521.

(26) Román, P.; Guzmán-Miralles, C.; Luque, A. *J. Chem. Soc., Dalton Trans.* **1996**, 3985.

(27) Decurtins, S.; Schmalle, H. W.; Pellaux, R.; Schneuwly, P.; Hauser, A. *Inorg. Chem.* **1996**, *35*, 1451.

(28) Decurtins, S.; Schmalle, H. W.; Pellaux, R.; Huber, R.; Fischer, P.; Ouladdiaf, B. *Adv. Mater.* **1996**, *8*, 647.

(29) Hernández-Molina, M.; Lloret, F.; Ruiz-Pérez, C.; Julve, M. *Inorg. Chem.* **1998**, *37*, 4131.

(30) Coronado, E.; Galán-Mascarós, J. R.; Gómez-García, C. J.; Martínez-Agudo, J. M. *Inorg. Chem.* **2001**, *40*, 113.

(31) (a) Tamaki, H.; Mitsumi, M.; Nakamura, K.; Matsumoto, N.; Kida, S.; Okawa, H.; Iijima, S. *Chem. Lett.* **1992**, 1975. (b) Decurtins, S.; Schmalle, H. W.; Pellaux, R.; Hauser, A. *Mol. Cryst. Liq. Cryst.* **1997**, *305*, 227.

(32) Armentano, D.; De Munno, G.; Lloret, F.; Palii, A.; Julve, M. *Inorg. Chem.* **2002**, *41*, 2007.

(33) Armentano, D.; De Munno, G.; Mastropietro, T. F.; Proserpio, D. M.; Lloret, F.; Julve, M. *Inorg. Chem.* **2004**, *43*, 5177.

(34) Armentano, D.; De Munno, G.; Mastropietro, T. F.; Lloret, F.; Julve, M. *J. Am. Chem. Soc.* **2005**, *127*, 10778.

$\{X_2[Fe_2(ox)_2Cl_4]\cdot pH_2O\}_n$ [X = $Me_2NH_2^+$ (**9**, $p = 1$), Me_3NH^+ (**10**, $p = 2$), and Me_4N^+ (**11**, $p = 0$)].[35]

Experimental Section

Materials. All chemicals were purchased from commercial sources and used as received without further purification. Elemental analyses (C, H, and N) were performed by the Microanalytical Service of the Università della Calabria.

Preparation of $\{X_2[Fe_2O(ox)_2Cl_2]\cdot pH_2O\}_n$ [X = Li^+ (1), Na^+ (2), and K^+ (3) with $p = 4$ and X = $MeNH_3^+$ (4), $Me_2NH_2^+$ (5), and $EtNH_3^+$ (6) with $p = 2$]. Compounds **1**−**6** were obtained as red rhombuses by slow evaporation at room temperature of an aqueous solution (10 mL) containing $FeCl_3$ (5 mmol), H_2ox (5 mmol), and XCl (5 mmol) [X = Li^+ (**1**), Na^+ (**2**), K^+ (**3**), $MeNH_3^+$ (**4**), $Me_2NH_2^+$ (**5**), and $EtNH_3^+$ (**6**)]. Suitable crystals for X-ray diffraction were obtained within 1 or 2 weeks. Yield: ca. 60–70 (**1** and **3**−**5**), 40 (**2**), and 20% (**6**). Anal. Calcd for $C_4H_8Cl_2Fe_2Li_2O_{13}$ (**1**): C, 10.43; H, 1.75. Found: C, 10.75; H, 1.36. Anal. Calcd for $C_4H_8Cl_2Fe_2Na_2O_{13}$ (**2**): C, 9.75; H, 1.64. Found: C, 10.00; H, 1.37. Anal. Calcd for $C_4H_8Cl_2Fe_2K_2O_{13}$ (**3**): C, 9.15; H, 1.54. Found: C, 9.43; H, 1.76. Anal. Calcd for $C_6H_{16}Cl_2Fe_2N_2O_{11}$ (**4**): C, 15.18; H, 3.40; N, 5.90. Found: C, 14.82; H, 3.95; N, 6.25. Anal. Calcd for $C_8H_{20}Cl_2Fe_2N_2O_{11}$ (**5**): C, 19.11; H, 4.01; N, 5.57. Found: C, 20.40; H, 3.75; N, 6.40. Anal. Calcd for $C_8H_{20}Cl_2Fe_2N_2O_{11}$ (**6**): C, 19.11; H, 4.01; N, 5.57. Found: C, 18.20; H, 3.60; N, 6.10. The water contents for **1**−**6** were confirmed by TGA.

Preparation of $\{X[Fe_2(OH)(ox)_2Cl_2]\cdot 2H_2O\}_n$ [X = $EtNH_3^+$ (7a) and $PrNH_3^+$ (8)] and $\{(H_3O)(EtNH_3)[Fe_2O(ox)_2Cl_2]\cdot H_2O\}_n$ (7b). Compounds **7a** and **8** were grown as yellow rhombic crystals by slow evaporation at room temperature of aqueous solutions (10 mL) containing $FeCl_3$ (5 mmol), H_2ox (5 mmol), and XCl (2.5 mmol) [X = $EtNH_3^+$ (**7a**) and $PrNH_3^+$ (**8**)] after 10 days. The deep-red compound **7b** is obtained from **7a** by an irreversible solid-to-solid transformation without any loss of crystallinity in 3 days. Yield: ca. 50 (**7a**) and 70% (**8**). Anal. Calcd for $C_6H_{13}Cl_2Fe_2NO_{11}$ (**7a**): C, 15.74; H, 2.86; N, 3.06. Found: C, 15.02; H, 3.05; N, 3.55. Anal. Calcd for $C_7H_{15}Cl_2Fe_2NO_{11}$ (**8**): C, 17.82; H, 3.20; N, 2.97. Found: C, 17.57; H, 3.58; N, 2.55. The formula of **7b** was determined by X-ray diffraction on single crystals. The water contents of **7a**, **7b**, and **8** were confirmed by TGA.

Preparation of $\{X_2[Fe_2(ox)_2Cl_4]\cdot pH_2O\}_n$ [X = $Me_2NH_2^+$ (9) with $p = 1$, Me_3NH^+ (10) with $p = 2$, and Me_4N^+ (11) with $p = 0$]. X-ray-quality yellow plates of compounds **9**−**11** were grown from aqueous solutions (10 mL) containing $FeCl_3$ (5 mmol), H_2ox (5 mmol), and XCl (5 mmol) [X = $Me_2NH_2^+$ (**9**), Me_3NH^+ (**10**), and Me_4N^+ (**11**)] after 3 days by slow evaporation at room temperature. The formation of red crystals of **5** occurred in the beaker where the synthesis of **9** was performed after 1 week of standing under ambient conditions. Yield: ca. 65–75% (**9**−**11**). Anal. Calcd for $C_8H_{18}Cl_4Fe_2N_2O_9$ (**9**): C, 17.80; H, 3.36; N, 5.19. Found: C, 18.02; H, 2.98; N, 5.45. Anal. Calcd for for $C_{10}H_{24}Cl_4Fe_2N_2O_{10}$ (**10**): C, 20.50; H, 4.13; N, 4.78. Found: C, 20.32; H, 3.95; N 4.35. Anal. Calcd for $C_{12}H_{24}Cl_4Fe_2N_2O_8$ (**11**): C, 24.94; H, 4.19; N, 4.85. Found: C, 24.63; H, 3.87; N, 4.51. TGA showed the loss of one and two crystallization water molecules per formula unit of **9** and **10**, respectively, in the temperature range 50–80 °C.

Physical Techniques. The IR spectra of the compounds were obtained with a Perkin-Elmer 1750 FTIR spectrophotometer in the 4000–400 cm^{-1} region. The UV–visible and TGA analyses were performed with a Perkin-Elmer Lambda 900 spectrophotometer and a Perkin-Elmer Pyris 6 TGA thermogravimetric analyzer, respectively. Variable-temperature (1.9–295 K) magnetic susceptibility and magnetization measurements on polycrystalline samples of **1**−**11** (amounting to ca. 11 mg) were carried out with a Quantum Design SQUID susceptometer using an applied magnetic field ranging from 100 G to 5 T. The alternating current (ac) measurements on polycrystalline samples of **1**−**11** were carried out at frequencies ranging from 33 to 1000 Hz with an ac field amplitude of 1 G and with lack of an external magnetic field. The experimental susceptibility data were corrected for the diamagnetic contribution of the constituent atoms and also for the sample holder.

X-ray Crystallographic Analysis. X-ray diffraction data were collected with a Bruker R3m/V automatic four-circle for compounds **4** and **9**–**11**, a Bruker Smart CCD for compound **2**, and a Xcalibur3 four-circle diffractometer for **11b**, whereas a Bruker Nonius APEX II CCD area detector diffractometer was used for the data collection of the remaining complexes (**1**–**3** and **5**–**8**). Graphite-monochromated Mo Kα radiation (α = 0.710 73 Å) was used in all cases. Lorentz−polarization and empirical absorption corrections through the Ψ-scan program[36] were applied for compounds **4** and **9**–**11**. The data for compounds **1**–**3** and **5**–**8** were processed through the *SAINT*[37] reduction and *SADABS*[38] absorption software. The structures were solved by direct methods and subsequently completed by Fourier recycling using the *SHELXTL* software package.[39] Several cations and water molecules in **1**−**11**, especially in the 3D family (**1**–**8**), show disorder because of the presence of large voids; consequently, only those not exhibiting any kind of disorder were refined anisotropically. Different peaks of electron density were found in the refinement of the structure of **2**, and they were assigned to a highly disordered sodium atom. No model for the water molecules of **2** was found. The hydrogen atoms of the water molecules in **3** were located on a ΔF map and refined with restraints, while those of the water molecules in **1** were not found. The $MeNH_3^+$ and $EtNH_3^+$ cations and the water molecules in **4** and **6** were located on a ΔF map, but their constituent atoms have very large thermal motions because of the disorder that they exhibit. For this reason, the atomic coordinates and the isotropic displacement parameters of the $MeNH_3^+$ cation and the water molecule in **4** as well as the carbon atoms of the $EtNH_3^+$ cation in **6** were not refined. A reasonable model for the disordered $Me_2NH_2^+$ cation and solvent molecules of **5** was not found. The contribution of the disordered cations of **5** to the diffraction pattern (16 molecules located in the voids of the channels of the lattice amounting to 43.7% of the unit cell) was subtracted from the observed data by

(35) (a) A preliminary communication of the structure of compound **11** was presented at the XV Symposium del Grupo Especializado de Cristalografía at Tenerife, Spain, in 2004 and at the E-MRS Spring Meeting, Strasbourg, France, in 2003. (b) During the preparation of the present paper, the crystal structure at room temperature and the variable-temperature magnetic study of this compound was published (Xu, H. B.; Wang, M. Z.; Gao, S. *Inorg. Chem.*, **2007**, web page, ic0618854). The authors observed a very weak spin canting at T_c = 3.8 K, which cannot be explained in the context of the centrosymetric space group it crystallizes. Because our magnetic measurements on this complex did not show the spin-canting phenomenon, we decided to check its centrosymmetric character at very low temperature (9.0 K in the present case).

(36) North, A. C. T.; Philips, D. C.; Mathews, F. S. *Acta Crystallogr., Sect. A* **1968**, *24*, 351.

(37) *SAINT*, version 6.45; Bruker Analytical X-ray Systems: Madison, WI, 2003.

(38) Sheldrick, G. M. *SADABS Program for Absorption Correction*, version 2.10; Analytical X-ray Systems: Madison, WI, 2003.

(39) *SHELXTL*; Bruker Analytical X-ray Instruments: Madison, WI, 1998.

Table 1. Crystal Data and Structure Refinement for Compounds **1**–**6**[a]

	1	**2**	**3**	**4**	**5**	**6**
empirical formula	$C_4H_8Cl_2Fe_2Li_2O_{13}$	$C_4H_8Cl_2Fe_2Na_2O_{13}$	$C_4H_8Cl_2Fe_2K_2O_{13}$	$C_6H_{16}Cl_2Fe_2N_2O_{11}$	$C_8H_{20}Cl_2Fe_2N_2O_{11}$	$C_8H_{20}Cl_2Fe_2N_2O_{11}$
T, K	100	293	100	293	293	293
fw	460.58	492.68	524.9	474.81	502.86	502.86
a, Å	14.8825(4)	14.986(4)	15.181(2)	14.956(7)	14.963(5)	14.779(1)
b, Å	23.328(1)	23.552(6)	23.807(2)	23.671(9)	23.345(8)	23.754(1)
c, Å	9.1087(4)	9.051(2)	8.640(1)	9.026(4)	9.317(3)	9.175(1)
V, Å^3	3162.4(2)	3195(1)	3122.5(5)	3195(2)	3255(2)	3220.9(3)
D_c, g cm^{-3}	1.935	1.749	2.233	1.974	1.905	2.074
μ, mm^{-1}	2.230	2.230	2.795	2.206	2.156	2.195
R1 [$I > 2\sigma(I)$][b]	0.0332	0.0459	0.0271	0.0611	0.0767	0.0297
wR2[c]	0.1017	0.1285	0.0688	0.1582	0.1750	0.0844

[a] Details in common: orthorhombic, *Fdd2*, and $Z = 8$. [b] $R1 = \sum||F_o| - |F_c||/\sum|F_o|$. [c] $wR2 = \{\sum[w(F_o^2 - F_c^2)^2]/[(w(F_o^2)^2]\}^{1/2}$. $w = 1/[\sigma^2(F_o^2) + (aP)^2 + bP]$ with $P = [F_o^2 + 2F_c^2]/3$, $a = 0.0751$ (**1**), 0.0959 (**2**), 0.0482 (**3**), 0.0888 (**4**), 0.1067 (**5**), and 0.0628 (**6**), and $b = 4.0489$ (**1**), 1.2225 (**2**), and 0 (**3**–**6**).

Table 2. Crystal Data and Structure Refinement for Compounds **7a**, **7b**, and **8**–**11**

	7a	**7b**	**8**	**9**	**10**	**11**	**11b**
empirical formula	$C_6H_{13}Cl_2Fe_2NO_{11}$	$C_6H_{13}Cl_2Fe_2NO_{11}$	$C_7H_{15}Cl_2Fe_2NO_{11}$	$C_8H_{18}Cl_4Fe_2N_2O_9$	$C_5H_{12}Cl_2FeNO_5$	$C_6H_{12}Cl_2FeO_4$	$C_6H_{12}Cl_2FeO_4$
T, K	100	100	293	293	293	293	9
cryst syst	monoclinic	orthorhombic	monoclinic	monoclinic	monoclinic	monoclinic	monoclinic
space group	C_c	*Fdd*2	C_c	$P2_1/c$	$P2_1/c$	$P2_1/c$	$P2_1/c$
Z	4	8	4	4	4	4	4
fw	457.77	457.77	471.80	539.74	292.91	288.92	288.92
a, Å	9.2090(5)	14.754(3)	9.644(2)	10.959(3)	8.133(2)	7.915(2)	7.888(2)
b, Å	14.712(1)	23.596(4)	14.747(3)	13.998(4)	8.588(2)	8.585(2)	8.534(2)
c, Å	12.518(1)	9.273(2)	12.310(2)	13.594(4)	17.729(4)	17.776(6)	17.496(4)
μ, deg	109.01(3)		108.46(1)	107.56(2)	91.18(3)	91.96(2)	91.17(3)
V, Å^3	1603.4(2)	3228(1)	1660.8(6)	1988(1)	1238.1(4)	1207.1(6)	1177.4(4)
D_c, g cm^{-3}	1.896	1.884	1.887	1.803	1.571	1.590	1.630
μ, mm^{-1}	2.193	2.178	2.120	2.037	1.645	1.681	1.723
R1 [$I > 2\sigma(I)$][a]	0.0331	0.0473	0.0665	0.0699	0.0513	0.0653	0.0707
wR2[b]	0.0824	0.1272	0.2297	0.1889	0.1399	0.1537	0.1661

[a] $R1 = \sum||F_o| - |F_c||/\sum|F_o|$. [b] $wR2 = \{\sum[w(F_o^2 - F_c^2)^2]/[(w(F_o^2)^2]\}^{1/2}$. $w = 1/[\sigma^2(F_o^2) + (aP)^2 + bP]$ with $P = [F_o^2 + 2F_c^2]/3$, $a = 0.0413$ (**7a**), 0.0906 (**7b**), 0.1596 (**8**), 0.1469 (**9**), 0.0867 (**10**), 0.1065 (**11**), and 0.0964 (**11b**), and $b = 12.3712$ (**7b**), 16.5554 (**8**), and 0.0000 (**7a**, **9**–**11**, and **11b**).

the "SQUEEZE" method as implemented in *PLATON*.[40] The final formulation of the compound is in agreement with the residual electron density and volume. A very good model for the $EtNH_3^+$ and solvent of compound **7a** was found in the refinement process, while a substantial amount of disordered solvent/counterions is present in the structure of compound **7b**. Consequently, the $EtNH_3^+$ cations were located on a ΔF map, but one of their atoms [C(3)] has a large thermal motion (0.21). Anyway, the isotropic displacement parameters were refined, but the atomic coordinates were refined with restraints. Although **7b** contains half a water molecule and half a hydronium cation per formula unit, only one oxygen atom with a large thermal motion (0.25) could be located in the structure because of disorder. Nevertheless, this peak was assigned to both species with a full-site occupancy. The hydrogen atoms of the water molecules of **7a** were located on a ΔF map and refined with restraints while those of the water molecules and/or H_3O^+ cations of **7b** were not found. The hydrogen atoms of the hydroxo bridge and the $EtNH_3^+$ cations in **7a** were set in calculated positions and refined as riding atoms, whereas the hydrogen atoms of the disordered $EtNH_3^+$ cations in **7b** were not located. The nitrogen atoms of the $Me_2NH_2^+$ cations in **9** are disordered in two positions; consequently, two peaks per cation were assigned with refined occupancy factors of 0.67 and 0.33, respectively, and no hydrogen atoms were defined. The hydrogen atoms of **10** and **11** were set in calculated positions and refined as riding atoms.

Full-matrix least-squares refinements on F^2 for all compounds were carried out by minimizing the function $\sum w(|F_o| - |F_c|)^2$, and they reached convergence with values of the discrepancy indices given in Tables 1 and 2. The final geometrical calculations were carried out with the *PARST97*[41a] program, whereas the graphical manipulations were performed with the *DIAMOND*[41b] program and the XP utility of the *SHELXTL* system. Crystallographic data are listed in Tables 1 (**1**−**6**) and 2 (**7a**−**11**). Selected bond lengths and angles are given in Tables 3 (**1**−**6** and **7a**), 4 (**7a** and **8**), 5 (**9**), and 6 (**10** and **11**). CCDC reference numbers are 225166, 244750, 244751 (**4**−**6**), 284328, 284329 (**7a** and **7b**), and 669724−669730 (**1**−**3**, **8**–**10**, and **11b**). See http://www.acs.org/suppdata/dt/xx/icxxxxxxx/ for crystallographic data in CIF or other electronic format.

Results and Discussion

Synthesis and Spectroscopic Characterization. A simple synthetic route to 1D (**9**−**11**) and 3D (**1**− **6**, **7a**, **7b**, and **8**) compounds containing oxalato (**1**−**11**), oxo (**1**−**6** and **7b**), and hydroxo bridges (**7a** and **8**) has been developed as outlined in Scheme 1. The reactions are clean, affording pure crystalline products in moderate yields. In this series, the discrimination between the formation and crystallization of either the 1D (oxalato bridge) or 3D (oxalato and oxo or hydroxo bridges) framework structures relies on the choice of the template cation, the crystallization time, and the oxalate-to-cation molar ratio. The right conditions for the selective preparation of the 1D or 3D networks were carefully established.

3D oxalato/oxo-bridged (**1**−**6**) and 1D oxalato-bridged (**9**−**11**) compounds were obtained as red rhombuses and yellow plates, respectively, from aqueous solutions containing $FeCl_3$, oxalic acid, and XCl in a 1:1:1 molar ratio (ca.

(40) (a) Spek, A. L. *Acta Crystallogr.* **1990**, *A46*, C34. (b) Van der Sluis, P.; Spek, A. L. *Acta Crystallogr.* **1990**, *A46*, 194.

Table 3. Selected Bond Distances (Å) and Angles (deg) for Compounds **1**–**6** and **7b**[a]

	X =						
	Li^+ (**1**)	Na^+ (**2**)	K^+ (**3**)	$MeNH_3^+$ (**4**)	$Me_2NH_3^+$ (**5**)	$EtNH_3^+$ (**6**)	$(H_3O)^+$ $(EtNH_3)^+$ (**7b**)
Fe(1)−O(1)	1.874(1)	1.801(2)	1.8037(9)	1.872(3)	1.817(5)	1.809(1)	1.825(3)
Fe(1)−O(2)	2.138(2)	2.184(3)	2.205(2)	2.162(5)	2.20(1)	2.201(2)	2.165(5)
Fe(1)−O(3)	2.039(2)	2.054(3)	2.060(1)	2.006(6)	2.01(1)	2.050(2)	2.056(5)
Fe(1)−O(4a)	2.128(2)	2.123(3)	2.127(1)	2.125(5)	2.119(9)	2.116(2)	2.121(5)
Fe(1)−O(5a)	2.037(2)	2.066(3)	2.053(1)	1.999(5)	1.99(1)	2.049(2)	2.052(5)
Fe(1)−Cl(1)	2.274(1)	2.325(1)	2.344(1)	2.290(2)	2.298(5)	2.321(1)	2.322(2)
O(1)−Fe(1)−O(5a)	101.31(8)	102.7(2)	103.49(7)	100.5(3)	102.1(4)	102.8(1)	102.2(3)
O(1)−Fe(1)−O(3)	92.28(9)	94.9(2)	95.85(7)	94.2(3)	94.8(5)	95.2(1)	93.6(3)
O(3)−Fe(1)−O(5a)	158.70(6)	156.6(1)	155.21(6)	158.6(2)	157.1(3)	156.25(7)	158.5(2)
O(1)−Fe(1)−O(4a)	89.08(5)	92.5(1)	93.27(4)	91.4(2)	92.5(3)	92.73(7)	92.0(2)
O(5a)−Fe(1)−O(4a)	79.11(6)	78.9(1)	78.94(5)	78.0(2)	79.0(4)	79.06(8)	79.6(2)
O(3)−Fe(1)−O(4a)	84.86(7)	85.1(1)	84.68(6)	86.2(2)	84.9(4)	84.76(8)	85.4(2)
O(1)−Fe(1)−O(2)	169.42(8)	171.7(2)	172.77(8)	170.6(3)	171.4(5)	172.1(1)	171.3(3)
O(2)−Fe(1)−O(5a)	85.55(6)	83.8(1)	82.98(6)	86.5(2)	85.2(4)	83.42(8)	84.4(2)
O(3)−Fe(1)−O(2)	78.95(6)	77.5(1)	77.06(5)	77.4(2)	77.0(4)	77.57(8)	78.7(2)
O(2)−Fe(1)−O(4a)	84.28(6)	83.4(1)	84.73(6)	83.9(2)	84.3(3)	83.63(8)	83.9(2)
O(1)−Fe(1)−Cl(1)	98.68(4)	98.35(7)	94.46(3)	96.9(1)	97.5(2)	97.95(5)	98.2(1)
O(5a)−Fe(1)−Cl(1)	92.40(5)	93.7(1)	94.67(4)	94.6(2)	93.4(3)	93.40(7)	92.5(2)
O(3)−Fe(1)− Cl(1)	100.73(6)	98.9(1)	98.45(4)	99.1(2)	99.7(3)	99.42(7)	99.8(2)
O(4a)−Fe(1)− Cl(1)	170.18(5)	168.0(1)	169.41(4)	169.8(2)	168.5(3)	168.10(7)	168.3(2)
O(2)−Fe(1)− Cl(1)	88.85(5)	86.4(1)	86.11(4)	88.8(2)	86.6(3)	86.39(7)	86.8(1)
Fe(1)−O(1)−Fe(1b)	133.6(2)	136.1(3)	135.4(1)	136.0(5)	136.6(8)	137.1(2)	136.0(5)

[a] Estimated standard deviations in the last significant digits are given in parentheses. Symmetry code: (a) $x - {}^1/_4, -y + {}^1/_4, z - {}^1/_4$; (b) $-x + 1, -y, z$.

Scheme 1

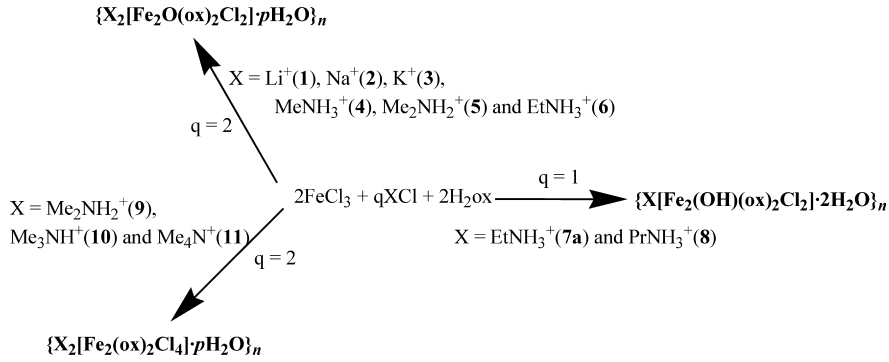

pH 2) depending on the speed of the evaporation and the nature of the cation. We could identify a borderline cation between the two types of compounds because the same cation ($Me_2NH_2^+$) allows the preparation of both of them by varying the evaporation time. In general, the 3D networks are obtained only with the smaller cations, whereas the chains are favored by the bulkier ones, such as Me_3NH^+ and Me_4N^+.

The 3D oxalato/hydroxo-bridged compounds **7a** and **8** are formed as yellow rhombuses from aqueous solutions in conditions similar to those of **1**−**6** by varying the iron(III)/oxalic acid/X molar ratio (2:2:1 instead of 1:1:1). It is noteworthy that only with the $EtNH_3^+$ cation both oxalato/hydroxo (**7a**) and oxalato/oxo (**6**) 3D species were obtained. All of our attempts to prepare oxalato/hydroxo compounds with other cations or the oxalato/oxo species with the $PrNH_3^+$ cation by varying the iron(III)/oxalic acid/X molar ratio were unsuccessful.

Remarkably, **7a** undergoes a solid-state transformation to yield another oxalato/oxo compound, namely, **7b**. This last compound differs from the parent complex **6** because of the occurrence of two types of univalent cations in the former (H_3O^+ and $EtNH_3^+$) versus only one in the latter ($EtNH_3^+$).

A similar behavior is not observed when the $PrNH_3^+$ cation is used (compound **8**). Significantly, the ethylammonium cation represents the borderline between the oxalato/oxo and oxalato/hydroxo 3D compounds.

The IR spectra of all compounds show two peaks in the range 3600–3100 cm^{-1}, which are due to the presence of crystallization water molecules (**1**−**10**) and the protonated alkylammonium cations (**4**−**10**). These absorptions are lacking in the IR spectrum of **11** given the anhydrous character of this compound together with the occurrence of Me_4N^+ as the cation. The occurrence of bisbidentate oxalate in all compounds is supported by the asymmetric (a broad peak in the range 1620–1670 cm^{-1}) and symmetric (a doublet in the range 1300–1350 cm^{-1}) O−C−O stretchings. A weak absorption in the frequency range 799–810 cm^{-1} in the IR spectra of **1**−**6**, **7a**, **7b**, and **8** is assigned to the asymmetric bending of the Fe−O−Fe bridging unit.[42] Significantly, an absorption band at ca. 1135 cm^{-1}, which may be reasonably

(41) (a) Nardelli, M. *J. Appl. Crystallogr.* **1995**, *28*, 659. (b) *DIAMOND*, version 2.1d; Crystal Impact GbR, CRYSTAL IMPACT K; Brandeburg & H. Putz GBR: Bonn, Germany, 2000.
(42) Nakamoto, K. *Infrared and Raman Spectra of Inorganic and Coordination Compounds*, 2nd ed.; Wiley: New York, 1970; p 168.

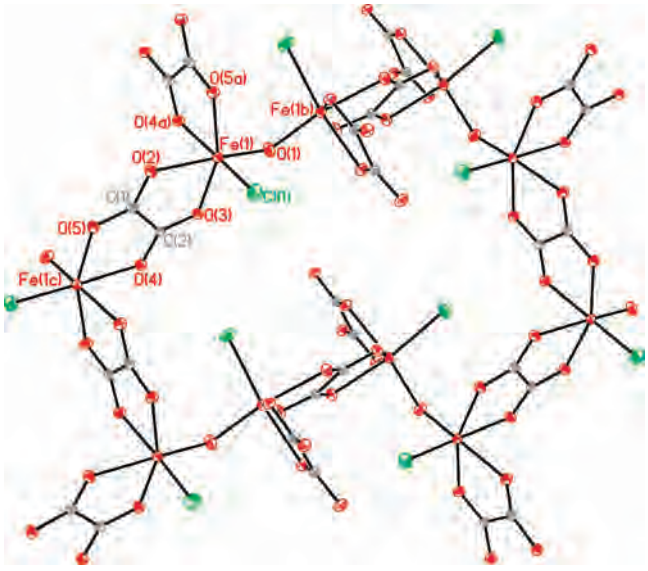

Figure 1. Perspective drawing of a decagon ring of the anionic 3D network of compounds **1**−**6** and **7b** showing the environment of the iron atoms. Symmetry code: (a) $x - {}^1/_4, -y + {}^1/_4, z - {}^1/_4$; (b) $-x + 1, -y, z$; (c) $x + {}^1/_4, {}^1/_4 - y, z + {}^1/_4$.

assigned to the Fe−O−H bending mode,[42] appears only in **7a** and **8**. The disappearance of this band upon transformation of **7a** into **7b** confirms the nature of the hydroxo (**7a**) and oxo (**7b**) bridges.

Diffuse-reflectance UV–visible spectra have been carried out on **7a** and **7b**. Their spectra show similar profiles. Three transitions at 330, 460, and 520 nm are observed in the spectrum of **7a**and are red-shifted (bands at 350, 470, and 550 nm) in that of **7b**. These values are similar to those of the charge-transfer and ligand-field transitions occurring in oxo-bridged iron(III) compounds.[43] The optical spectra of the diiron(III) core are usually sensitive to the protonation of the oxo bridge to form hydroxo species. So, the observed shift is most likely due to protonation of the oxo bridge.

Description of the Structures. $\{X_2[Fe_2O(ox)_2Cl_2]\cdot pH_2O\}_n$ for X = Li^+ (1), Na^+ (2), and K^+ (3) (p = 4) and $MeNH_3^+$ (4), $Me_2NH_2^+$ (5), and $EtNH_3^+$ (6) (p = 2). The structures of compounds **1–6** are made up of the anionic oxo- and oxalato-bridged iron(III) 3D network $[Fe_2O(ox)_2Cl_2]^{2-}$ (**1**−**6** [see Figure 1], alkaline (**1–3**), or ammonium derivative (**4–6**) cations and crystallization water molecules (**1**−**6**). No significant structural modifications have been produced in the networks with this series of univalent cations; hence, all of the cited complexes show an open framework that is analogous to that found in the parent ammonium compound.[20] The cohesion of the crystal lattice is ensured by electrostatic interactions, as well as hydrogen bonds involving the counterions, the oxalate groups, the coordinated chlorine atoms, and the crystallization water molecules.

Each iron atom exhibits a distorted octahedral environment, being bonded to four oxygen atoms of two cis oxalate groups [O(2)O(3)O(4a)O(5a) set of atoms; (a) $x - {}^1/_4, -y + {}^1/_4, z - {}^1/_4$], one oxygen atom of the oxo group [O(1)], and one chlorine atom [Cl(1)]. The values of the Fe−O(ox) [1.999(5)−2.205(2) Å] and Fe−O(μ-oxo) [1.801(2)−1.874(1) Å] bond lengths (Table 3) are in agreement with those reported in the literature for other oxalato-[32–34,44] and oxo-bridged[32–34,45] iron(III) complexes. The value of the Fe−Cl bond distance [2.274(1)−2.344(1) Å; Table 3] compares well with those reported for other chloride-containing iron(III) complexes.[32–34,44c,45d,46] The best equatorial plane around the iron atom is defined by the O(2)Cl(1)O(4a)O(5a) set of atoms [largest deviation from the mean plane is 0.098(1) Å at O(4a) in **3**]. The greater displacement for the metal atom from this plane [ca. 0.268(1) Å] is observed in **3**. The reduced value of the bite angle of the bischelating oxalate ligand [the values of the O(3)−Fe(1)−O(2) and O(4a)−Fe(1)−O(5a) bond angles varying between 77.06(5) (**3**) and 79.11(6)° (**1**); Table 3] is the main factor accounting for the distortion of the metal environment from the ideal octahedral geometry.

The Fe−O−Fe linkage is not linear, with the values of angles at the oxo bridge varying in the range 133.6(2)−137.1(2)° (see Table 7). The value of 133.6(2)° observed in **1** is the shortest one reported so far for this type of bridge [previous values ranging from 139 to 180°].[45] The values of the iron−iron separation through the single oxo bridge and through the bisbidentate oxalato are listed in Table 7.

The 3D network can be described as oxalato-bridged iron(III) chains growing in the direction of the diagonal line of the a and c axes that are linked through a single oxo bridge to parallel planes containing only oxalato-bridged iron(III) chains (see Figure 2a). The dihedral angle between the planes and the chains is ca. 60°. These motifs define helical tunnels (dimensions of ca. 15.7 × 8.7 Å^2), as shown in Figure 2b. Two subunits, each one being constituted of three iron atoms and two ox groups, that are linked to two others that contain only two iron atoms and one ox group by means of four oxo bridges build a pseudohexagonal motif. The alkaline (**1**−**3**) and alkylammonium (**4**−**6**) cations with the crystallization water molecules are placed in these tunnels, and they are held together by means of hydrogen bonds (see Figure 2b as an illustrative example).

The positions of the cations and water molecules were found only in compounds **1** and **3**. It is important to note that the arrangement of the cations and water molecules within the channels is different for these two compounds.

(43) (a) Turowski, P. N.; Armstrong, W. H.; Liu, S.; Brown, S. N.; Lippard, S. J. *Inorg. Chem.* **1994**, *33*, 636. (b) Wu, F. J.; Kurtz, D. M.; Hagen, K. S.; Nyman, P. D.; Debrunner, P. G.; Vankai, V. A. *Inorg. Chem.* **1990**, *29*, 5174. (c) Vankai, V. A.; Newton, M. G.; Kurtz, D. M. *Inorg. Chem.* **1992**, *31*, 341.

(44) (a) Triki, S.; Bérézovsky, F.; Sala Pala, J.; Coronado, E.; Gómez-García, C. J.; Clemente, J. M.; Riou, A.; Molinié, P. *Inorg. Chem.* **2000**, *39*, 3771. (b) Armentano, D.; De Munno, G.; Lloret, F.; Julve, M. *CrystEngComm* **2005**, *7*, 57. (c) Feist, M.; Troyanov, S.; Kemnitz, E. *Inorg. Chem.* **1996**, *35*, 3067. (d) Armentano, D.; De Munno, G.; Mastropietro, T. F.; Lloret, F.; Julve, M. *Chem. Commun.* **2004**, 1160. (e) Armentano, D.; De Munno, G.; Faus, J.; Lloret, F.; Julve, M. *Inorg. Chem.* **2001**, *40*, 655.

(45) (a) Murray, S. *Coord. Chem. Rev.* **1974**, *12*, 1. (b) Kurtz, D. M. *J. Chem. Rev.* **1990**, *90*, 585. (c) Matsushima, H.; Iwasawa, K.; Ide, K.; Reza, M. Y.; Koikawa, M.; Tokii, T. *Inorg. Chim. Acta* **1998**, *274*, 224. (d) Xiang, D. F.; Tan, X. S.; Zhang, S. W.; Han, Y.; Yu, K. B.; Tang, W. X. *Polyhedron* **1998**, *17*, 2095.

(46) De Munno, G.; Ventura, W.; Viau, G.; Lloret, F.; Faus, J.; Julve, M. *Inorg. Chem.* **1998**, *37*, 1458.

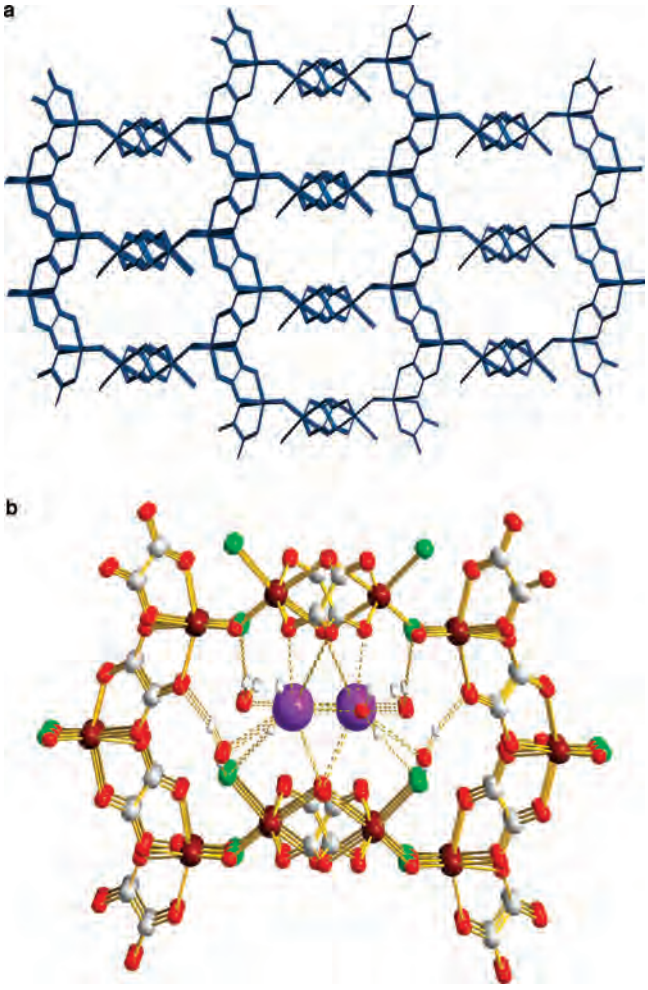

Figure 2. (a) View of a fragment of the 3D anionic network of compounds **1**−**6** and **7b** along the diagonal of the crystallographic *a* and *c* axes. Cations and crystallization water molecules have been omitted for clarity. (b) View of the pseudohexagonal motif in **3** showing the hydrogen bonds as broken lines.

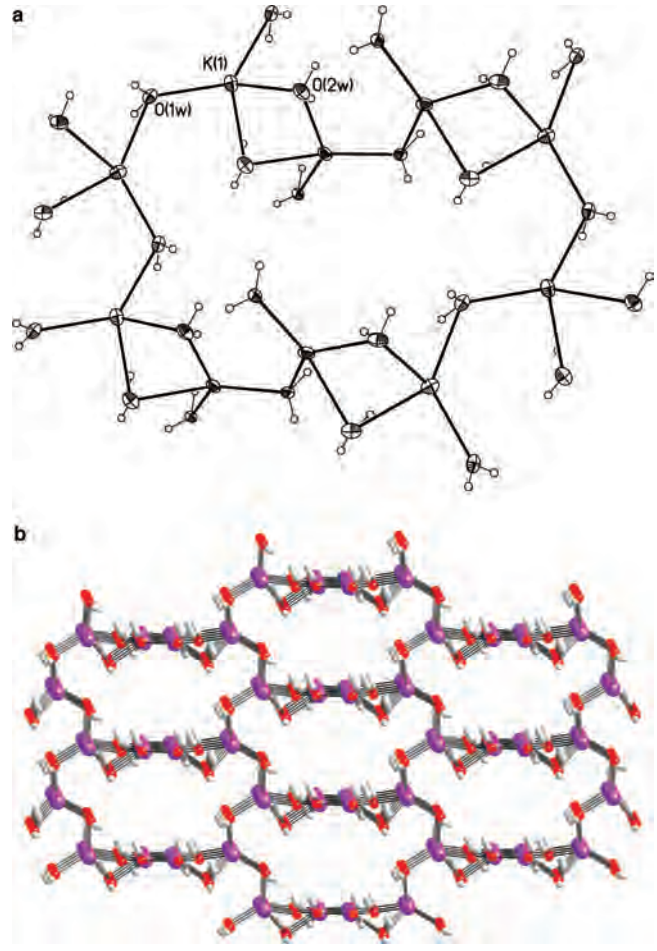

Figure 3. (a) View of the decagon ring in **3** defined by the $K^+\cdots O_w$ interactions. (b) Perspective view showing a 3D-connected net of K^+, interpenetrating with the iron(III) atoms 3D net.

Only one interaction between the alkaline cation and a water molecule [Li(1)−O(1w) = 2.54(2) Å] could be established in **1**. As far as the hydrogen bonds are concerned, the O(1w) and O(2w) water molecules interact with each other [O(2w)···O(1w) = 2.95(2) Å] and they are linked to the anionic 3D network by means of hydrogen bonds involving the coordinated chloride ion and two oxygen atoms of the oxalate groups [O(1w)···O(2) = 2.93(1) Å, O(2w)···O(5) = 2.904(7) Å, and O(2w)···Cl(1e) = 3.396(8) Å; (e) $-x + {}^3/_4 + 1$, $y + {}^1/_4$, $z - {}^1/_4$]. On the contrary, each potassium atom in **3** interacts with four water molecules, with two of them acting as double [K(1)−O(2w) = 2.780(1) Å and K(1)−O(2wf) = 2.808(1) Å; (f) $-x + {}^3/_2$, $-y + {}^1/_2$, $+z$] and the other two as single [K(1)−O(1w) = 2.746(1) Å and K(1)−O(1wa) = 2.794(1) Å] bridges (Figure 3a). These interactions give rise to a 3D cationic network that is interpenetrated with the 3D anionic iron(III) net (Figure 3b). Taking into account the connectivity of the iron or potassium atoms, the overall structure can be described as two interpenetrating three-connected decagon nets ($10_2.10_4.10_4$), and accordingly it may be considered as the three-connected analogue of the $ThSi_2$ net.[47] The cationic and anionic 3D networks are linked to each other by means of hydrogen bonds, involving water molecules, oxalate oxygens, and coordinated chloride anions [3.205(2), 3.089(3), and 3.465(3) Å for O(1w)···Cl(1), O(2w)···O(3g), and O(2w)···Cl(1a), respectively; (g) ${}^5/_4 - x$, ${}^1/_4 + y$, $z + {}^1/_4$] and weak $K^+\cdots$O(ox) interactions [2.894(1), 2.917(1), and 3.002(1) Å for K(1)···O(2), K(1)···O(3h), and K(1)···O(4i), respectively; (h) ${}^1/_4 + x$, ${}^1/_4 - y$, $z - {}^3/_4$; (i) x, y, $z - 1$].

$\{X[Fe_2(OH)(ox)_2Cl_2]\cdot 2H_2O\}_n$ [X = $EtNH_3^+$ (7a) and $PrNH_3^+$ (8)] and $\{(H_3O)(EtNH_3)[Fe_2O(ox)_2Cl_2]\cdot 2H_2O\}_n$ (7b). Compounds **7a** and **8** show a 3D open MOF basically analogous to that found in the previous compounds **1–6** (Figure 4), with the cations located in the anionic cages comprising as the only difference the presence of an hydroxo bridge instead of the oxo one, which merely causes slight modifications in the 3D framework (Figure 5). Unlike the alkylammonium-containing oxo-bridged compounds, it was possible to determine the positions of the cations and water molecules in **7a** and **8**. Compound **7a** retains its framework and single crystallinity upon a proton-transfer reaction that

(47) (a) Carlucci, L.; Ciani, G.; Proserpio, D. M.; Sironi, A. *J. Am. Chem. Soc.* **1995**, *117*, 4562. (b) Yaghi, O. M.; Li, H. *J. Am. Chem. Soc.* **1996**, *118*, 295. (c) O'Keeffe, M.; Eddaoudi, M.; Li, H.; Reineke, T.; Yaghi, O. M. *Solid State Chem. J.* **2000**, *152*, 3.

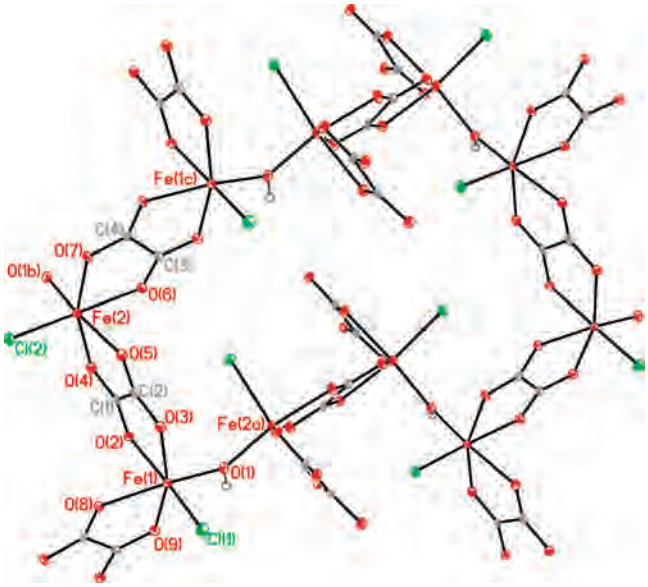

Figure 4. ORTEP drawing of a decagon ring of the anionic 3D network of **7a** and **8**. Thermal ellipsoids are drawn at the 30% probability level. Symmetry code: (a) $x - {}^1/_2, -y + {}^1/_2, z - {}^1/_2$; (b) $x + {}^1/_2, -y + {}^1/_2, -z + 1$; (c) $x + {}^1/_2, y + {}^1/_2, z$.

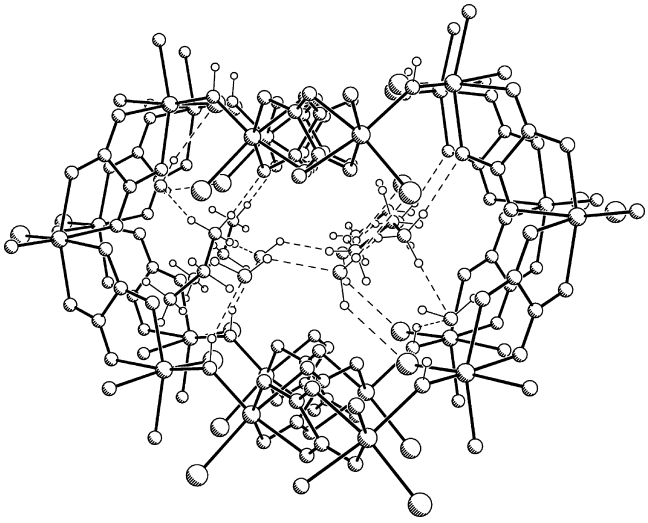

Figure 5. View of the pseudohexagonal motif in **7a** showing the hydrogen bonds as broken lines.

occurs within the net, leading to the new species **7b**, where the hydroxo group is transformed into an oxo one and a water molecule is protonated. Compound **8**, containing the $PrNH_3^+$ cation, seems to be more stable, and no solid reaction was observed.

Each iron atom in **7a**, **7b**, and **8** is in a distorted octahedral environment, being bonded to four oxygen atoms from two cis oxalate groups, a chlorine atom, and one oxygen atom of either one hydroxo (**7a** and **8**) or oxo groups (**7b**). The larger structural modifications when comparing **7a** and **8** with **7b** concern the values of the angles at the hydroxo (**7a** and **8**) and oxo (**7b**) bridges, which are more bent in the former case [132.4(2)° (**7a**) and 133.7(4)° (**8**) versus 136.0(5)° (**7b**)], and the Fe−O(bridge) bond length, which is shorter in the latter one [1.984(3) and 1.882(3) Å for **7a**, 1.825(3) Å for **7b**, and 1.934(7) and 1.926(6) Å for **8**]. The values of the Fe−O(hydroxo) bond length in **7a** and **8** agree with those

Table 4. Selected Bond Distances (Å) and Angles (deg) for Compounds **7a** and **8**[a]

	X =	
	$EtNH_3^+$ (**7a**)	$PrNH_3^+$ (**8**)
Fe(1)−O(1)	1.984(3)	1.934(7)
Fe(1)−O(2)	2.076(3)	2.121(6)
Fe(1)−O(3)	2.050(3)	2.063(7)
Fe(1)−O(8)	2.161(3)	2.094(6)
Fe(1)−O(9)	2.017(3)	2.054(7)
Fe(1)−Cl(1)	2.221(1)	2.257(2)
Fe(2)−O(1b)	1.882(3)	1.926(6)
Fe(2)−O(4)	2.074(3)	2.049(7)
Fe(2)−O(5)	2.067(3)	2.129(6)
Fe(2)−O(6)	2.150(3)	2.097(7)
Fe(2)−O(7)	2.035(3)	2.030(7)
Fe(2)−Cl(2)	2.314(1)	2.265(3)
O(1)−Fe(1)−O(9)	86.0(1)	92.7(3)
O(1)−Fe(1)−O(3)	104.2(1)	97.8(3)
O(9)−Fe(1)−O(3)	162.8(1)	162.3(2)
O(1)−Fe(1)−O(2)	92.4(1)	88.2(3)
O(9)−Fe(1)−O(2)	89.3(1)	87.2(3)
O(3)−Fe(1)−O(2)	76.6(1)	79.0(2)
O(1)−Fe(1)−O(8)	168.6(1)	169.5(3)
O(9)−Fe(1)−O(8)	83.2(1)	80.2(3)
O(3)−Fe(1)−O(8)	85.5(1)	87.3(3)
O(2)−Fe(1)−O(8)	83.9(1)	83.8(3)
O(1)−Fe(1)−Cl(1)	96.6(1)	99.4(2)
O(9)−Fe(1)−Cl(1)	98.9(1)	99.5(2)
O(3)−Fe(1)−Cl(1)	93.79(9)	92.9(2)
O(2)−Fe(1)−Cl(1)	168.2(1)	169.6(2)
O(8)−Fe(1)−Cl(1)	88.62(9)	89.4(2)
O(1b)−Fe(2)−O(7)	94.9(1)	100.7(3)
O(1b)−Fe(2)−O(5)	168.9(1)	166.8(3)
O(7)−Fe(2)−O(5)	89.8(1)	90.7(3)
O(1a)−Fe(2)−O(4)	95.7(1)	88.3(3)
O(7)−Fe(2)−O(4)	160.2(1)	163.3(3)
O(5)−Fe(2)−O(4)	77.1(1)	79.0(3)
O(1b)−Fe(2)−O(6)	87.4(1)	91.9(3)
O(7)−Fe(2)−O(6)	82.3(1)	79.3(3)
O(5)−Fe(2)−O(6)	83.3(1)	83.8(3)
O(4)−Fe(2)−O(6)	81.6(1)	86.5(3)
O(1b)−Fe(2)−Cl(2)	99.4(1)	95.7(2)
O(7)−Fe(2)−Cl(2)	91.3(1)	90.9(2)
O(5)−Fe(2)−Cl(2)	90.5(1)	90.6(2)
O(4)−Fe(2)−Cl(2)	103.4(1)	102.2(2)
O(6)−Fe(2)−Cl(2)	171.0(1)	168.5(2)
Fe(1)−O(1)−Fe(2a)	132.4(2)	133.7(4)

[a] Estimated standard deviations in the last significant digits are given in parentheses. Symmetry code: (a) $x - {}^1/_2, -y + {}^1/_2, z - {}^1/_2$; (b) $x + {}^1/_2, -y + {}^1/_2, -z + 1$.

reported in the literature for other iron(III) hydroxo compounds.[48] On the contrary, the Fe−O(oxo) bonds in **7b** are longer than those usually observed for other iron(III) oxo complexes.[45] As far as the Fe−O(ox) bond distances are concerned [values varying in the range 2.017(3)−2.165(5) Å; Table 4], they agree with those reported in the literature for other oxalato-bridged iron(III) complexes[32–34,44] and with the other reported analogous compounds **1**–**6**. Also, the Fe−Cl bond lengths [values covering the range 2.265(3)−2.322(2) Å] are in agreement with those reported for other similar compounds.[32–34,44c,45d]

(48) (a) Armstrong, W. H.; Lippard, S. *J. Am. Chem. Soc.* **1984**, *106*, 4632. (b) Scheidt, W. R.; Beisong, C.; Safo, M. K.; Cukiernik, F.; Marchon, J.-C.; Debrunner, P. G. *J. Am. Chem. Soc.* **1992**, *114*, 4420. (c) Evans, D. R.; Mathur, R. S.; Heerwegh, K.; Reed, C. A.; Xie, Z. *Angew. Chem., Int. Ed. Engl.* **1997**, *36*, 1335. (d) Hung, C.-H.; Chen, W.-C.; Lee, G.-H.; Peng, S.-M. *Chem. Commun.* **2002**, 1516. (e) Alam, M. A.; Nethaji, M.; Ray, M. *Inorg. Chem.* **2005**, *44*, 1302.

The best equatorial planes around the iron atoms in **7a** and **8**are defined by the Cl(1)O(2)O(3)O(9) [at Fe(1)] and Cl(2)O(4)O(6)O(7) [at Fe(2)] sets of atoms [the largest deviation from the mean plane is 0.049(2) Å at O(6) in compound **7a**]. The greater displacement of the iron atom from these planes is observed for Fe(2) in **7a** [0.177(2) Å]. The equatorial plane around the iron atom in **7b** may be defined by the Cl(1)O(2)O(3)O(4) set of atoms [largest deviation from the mean plane is only 0.062(2) Å at O(3)], and the metal atom is 0.242(2) Å out of this plane. The reduced value of the bite angle of the oxalato ligand in **7a**, **7b**, and **8** [values varying in the range 76.6(1)−83.2(1)°] is the main source of distortion of the iron environment from the ideal octahedral geometry.

The values of the iron−iron separation through the single hydroxo (**7a** and **8**) or oxo (**7b**) bridges as well as those through the bridging oxalato are listed in Table 7.

A general mechanism was postulated for this solid–solid transformation based on a proton transfer from the hydroxo bridge to a water molecule with a subsequent opening of the Fe−O−Fe angle without the channel framework collapsing. This assumption is supported by the occurrence of an intermolecular hydrogen bond in **7a**, which involves a water molecule behaving as both an acceptor toward an hydroxo group [2.82 Å for O(1)−H···O(2w)] and a donor toward a second water molecule [2.76 Å for O(2w)−H(4w)···O(1w)]. Furthermore, the water molecules act as acceptors toward the ethylammonium cations [2.96 and 2.79 Å for N(1)···O(1w) and N(1)···O(2w), respectively], and they are attached to the net through interactions with the chloro atoms [3.51 Å for O(1w)···Cl(1) and O(1w)···Cl(2)]. Moreover, we have noted that the dehydration inhibits the crystal-to-crystal transformation. If the yellow compound is completely dehydrated, the transformation occurs more slowly, probably after a rehydration process, demonstrating the key role played by the crystallization water molecules. The proton transfer is followed by a disordered rearrangement of cations and water molecules probably induced by the repulsive interactions between the H_3O^+ and $EtNH_3^+$ cations. No more oxygen atoms of water molecules/hydronium cations are close to the oxo bridge in the red phase (as occurs in **7a** for the hydroxo group) being substituted by the $-NH_3^+$ group of the ethylammonium cation. It deserves to be pointed out that the space group of the resulting red phase (**7b**) is identical with that of the related family **1**–**6**, where two cations are present. Although a similar network of hydrogen bonds has been observed in compound **8**, no transformation occurs in this compound. Most likely, the greater stability of the yellow phase for this compound is due to a minor flexibility of the net in rearranging a bulkier cation.

$\{X_2[Fe_2(ox)_2Cl_4]\cdot pH_2O\}_n$ for X = $Me_2NH_2^+$ (9, p = 1), $Me_3NH_2^+$ (10, p = 2), and Me_4N^+ (11, p = 0). The structures of the compounds **9**−**11** are made up of $[Fe_2(ox)_2Cl_4]^{2-}$ anionic chains, dimethyl- (**9**), trimethyl- (**10**), and tetramethylammonium (**11**) cations, and crystallization water molecules (**9** and **10**). The iron atoms of these compounds

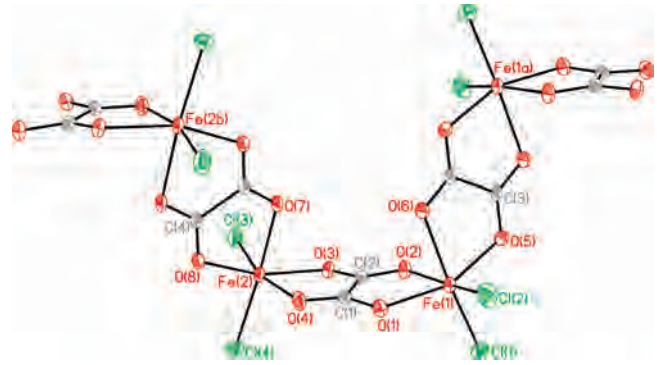

Figure 6. ORTEP drawing of a fragment of the chain motif in **9**. Symmetry code: (a) 1 − x, −y, 1 − z; (b) 1 − x, −y, 2 − z.

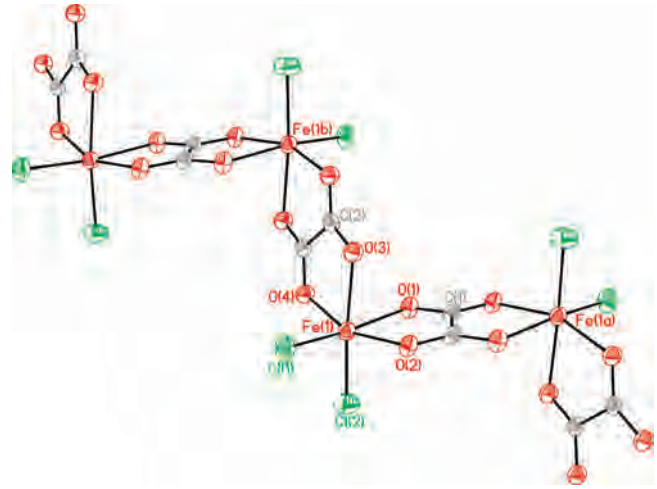

Figure 7. ORTEP drawing of a fragment of the zigzag chain in **10** and **11**. Symmetry code: (a) −x, 1 − y, −z; (b) −x, 2 − y, −z.

are bridged by bisbidentate oxalate groups, with two chlorine atoms acting as terminal ligands. Electrostatic interactions (**9**−**11**), as well as hydrogen bonds involving the counterions, the oxalate groups, the coordinated chlorine atoms, and the crystallization water molecules (**9** and **10**), ensure the cohesion of the crystal lattice. A fragment of the anionic motif with the atom-numbering scheme is shown in Figures 6 (**9**) and 7 (**10** and **11**). Recently, oxalate-bridged iron(III) chains containing terminal chlorine atoms have been reported.[35b,49] One of them is compound **11**, whose structure (solved at room temperature) and magnetic properties were the subject of a recent report.[35] Here we present its structure but solved at 9.0 K (**11b**) in order to give a clear-cut answer to the occurrence of spin canting in this compound (see the magnetic discussion). No significant differences have been found in the two structures solved at room temperature and at 9 K, as shown in Tables 2 and 6.

Two crystallographically independent iron atoms occur in the asymmetric unit in **9**, while only one is present in the isostructural compounds **10** and **11** because of the inversion center located at the middle of the C−C bond in the ox group. Each iron atom in **9**−**11** is in a distorted octahedral

(49) (a) Zhang, B.; Wang, T.; Fujiwara, H.; Kobayashi, H.; Kurmoo, M.; Inoue, K.; Mori, T.; Gao, S.; Zhang, Y.; Zhu, D. *Adv. Mater.* **2005**, *17*, 1988–1991. (b) Zhang, B.; Wang, T.; Zhang, Y.; Takahashi, K.; Okano, Y.; Cui, H.; Kobayashi, H.; Kurmoo, M.; Inoue, K.; Pratt, F. L.; Zhu, D. *Inorg. Chem.* **2006**, *45*, 3275.

Table 5. Selected Bond Distances (Å) and Angles (deg) for Compound **9**[a]

	X = $Me_2NH_2^+$ (**9**)
Fe(1)−O(1)	2.058(4)
Fe(1)−O(2)	2.129(4)
Fe(1)−O(5)	2.054(4)
Fe(1)−O(6)	2.167(4)
Fe(1)−Cl(1)	2.247(2)
Fe(1)−Cl(2)	2.252()
Fe(2)−O(3)	2.065(4)
Fe(2)−O(4)	2.118(5)
Fe(2)−O(7)	2.171(4)
Fe(2)−O(8)	2.030(4)
Fe(2)−Cl(3)	2.283(2)
Fe(2)−Cl(4)	2.239(2)
O(5)−Fe(1)−O(1)	158.2(2)
O(5)−Fe(1)−O(2)	88.4(2)
O(1)−Fe(1)−O(2)	79.1(2)
O(5)−Fe(1)−O(6)	77.4(2)
O(1)−Fe(1)−O(6)	83.1(2)
O(2)−Fe(1)−O(6)	81.2(2)
O(5)−Fe(1)−Cl(1)	93.7(1)
O(1)−Fe(1)−Cl(1)	104.1(1)
O(2)−Fe(1)−Cl(1)	90.4(1)
O(6)−Fe(1)−Cl(1)	168.8(1)
O(5)−Fe(1)−Cl(2)	98.0(1)
O(1)−Fe(1)−Cl(2)	91.2(1)
O(2)−Fe(1)−Cl(2)	167.1(1)
O(6)−Fe(1)−Cl(2)	89.3(1)
Cl(1)−Fe(1)−Cl(2)	100.24(8)
O(8)−Fe(2)−O(3)	159.0(2)
O(8)−Fe(2)−O(4)	91.1(2)
O(3)−Fe(2)−O(4)	78.9(2)
O(8)−Fe(2)−O(7)	78.2(2)
O(3)−Fe(2)−O(7)	82.1(2)
O(4)−Fe(2)−O(7)	82.0(2)
O(8)−Fe(2)−Cl(4)	93.2(1)
O(3)−Fe(2)−Cl(4)	105.4(1)
O(4)−Fe(2)−Cl(4)	91.6(1)
O(7)−Fe(2)−Cl(4)	169.0(1)
O(8)−Fe(2)−Cl(3)	97.8(1)
O(3)−Fe(2)−Cl(3)	89.1(1)
O(4)−Fe(2)−Cl(3)	165.9(1)
O(7)−Fe(2)−Cl(3)	89.2(1)
Cl(4)−Fe(2)−Cl(3)	98.67(8)

[a] Estimated standard deviations in the last significant digits are given in parentheses.

environment, being bonded to four oxygen atoms of two cis oxalate groups and to two chlorine atoms. The Fe−O(ox) [values varying in the range 2.019(5)−2.171(4) Å] and Fe−Cl bond lengths [values varying in the range 2.219(2)−2.283(2) Å] are in agreement with those reported in the previous family. The best equatorial planes around the Fe(1) and Fe(2) atoms in **9** are defined by the O(1)Cl(1)O(5)O(6) and O(7)Cl(4)O(3)O(8) sets of atoms, respectively [the largest deviation from the mean plane is 0.014 (2) Å at O(6)], with the metal atoms being 0.187(2) [Fe(1)] and 0.146(2) Å [Fe(2)] out of these planes. The O(2)Cl(2)O(3)O(4) set of atoms defines the equatorial plane in **10** and **11** [with the largest deviations from the mean plane being 0.035(2) Å (**10**) and 0.014(2) Å (**11**) at O(3)]. The iron atom is shifted by 0.235(2) Å (**10**) and 0.195(2) Å (**11**) from these planes. The main distortion from the ideal octahedral geometry of the metal environment is due to the reduced bite angle of the oxalate ligand [values varying in the range 77.4(2)−79.1(2) Å], as previously observed in compounds **1**−**8**.

The iron−iron separation through the three crystallographically independent oxalate ligands in compound **9** are 5.439(2) [Fe(1)···Fe(2)], 5.514(2) [Fe(1)···Fe(1a); (a) $1 - x, -y, 1 - z$], and 5.492(2) Å [Fe(2)···Fe(2b); (b) $1 - x, -y, 2 - z$], values that compare well with those observed in **10** [5.460(1) and 5.482(1) Å] and **11** [5.455(2) and 5.469(2) Å] for Fe(1)···Fe(1a) and Fe(1)···Fe(1b) [(a) $-x, 1 - y, -z$; (b) $-x, 2 - y, -z$]. The main structural difference between **9** and **10** and **11** concerns the arrangement of the chains in the packing. The oxalate groups in **9** produce a chain motif developing along the *z* axis and focusing on the oxalate that bridges the Fe(1) and Fe(2) atoms: the Cl(1) and Cl(4) atoms are in cis positions, and the Cl(2) and Cl(3) ones are in trans positions; however, for the other two oxalate bridges in **9**, the chloride atoms on adjacent iron atoms are in trans positions. To the best of our knowledge, a similar motif has been observed only in an oxalate-bridged heterobimetallic chain.[50] On the contrary, the oxalate groups in **10** and **11** produce a *zigzag* chain motif developing along the *y* axis with the chloro atoms of adjacent iron atoms in a trans arrangement (Figure 7).

The dimethylammonium cations in **9** are linked to the chains by means of hydrogen bonds, directly [N(1)···O(6)] or through crystallization water molecules [N(2)···O(9)···O(4)]. Adjacent chains are linked by means of hydrogen bonds involving water molecules [O(9)···Cl(1)] and the dimethylammonium cations [N(1)···Cl(3) and N(1)···Cl(1)] (see Figures S1 and S2 in the Supporting Information). Hydrogen bonds involving trimethylammonium cations, crystallization water molecules, oxalate oxygen atoms, and chlorine atoms occur also in **10**, as shown in Figure 8, leading to a layered structure. On the contrary, the adjacent chains in **11** are linked only by means of weak C−H(methyl)···O(ox)- and C−H(methyl)···Cl-type interactions (Figure 9).

Magnetic Properties. The description and discussion of the magnetic properties of the 1D compounds **9**−**11** will be performed first for pedagogic reasons, and then the more complicated magnetic behavior of the spin-canted 3D compounds **1**−**8** will close the present work.

1D Oxalate-Bridged Compounds. The magnetic properties of **9**−**11** as both χ_M and $\chi_M T$ versus *T* plots [χ_M is the magnetic susceptibility per one iron(III) ion] under an external magnetic field of 1 T ($T \geq 100$ K) and 100 G ($T < 100$ K) are shown in Figures 10 (**9**), S3 (**10**) and S4 (**11**) in the Supporting Information. At room temperature, $\chi_M T$ is equal to 3.45 (**9** and **11**) and 3.70 $cm^3\ mol^{-1}\ K$ (**10**), values that are somewhat below that expected for a magnetically isolated spin sextet ($\chi_M T = 4.375\ cm^3\ mol^{-1}K$ with $g = 2.0$). Upon cooling, $\chi_M T$ continuously decreases and it practically vanishes at 1.9 K. A maximum of the magnetic susceptibility is observed at 49 (**9**), 40 (**10**), and 48 K (**11**) These features are characteristic of a relatively large antiferromagnetic coupling between the local spin sextuplets.

(50) Coronado, E.; Galán-Mascarós, J. R.; Gómez-García, C. J.; Martí-Gastaldo, C. *Inorg. Chem.* **2005**, *44*, 6197.

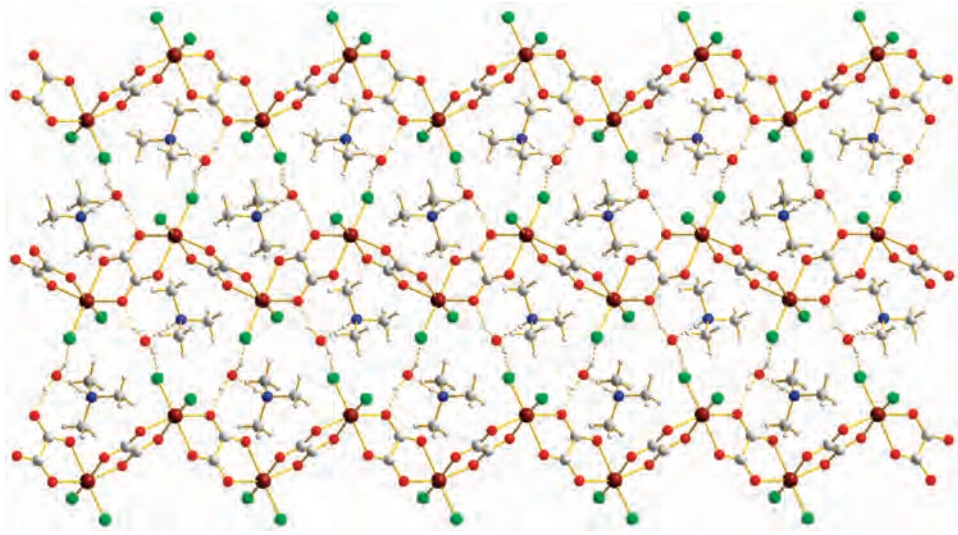

Figure 8. View along the *x* axis showing the supramolecular motif in compound **10**.

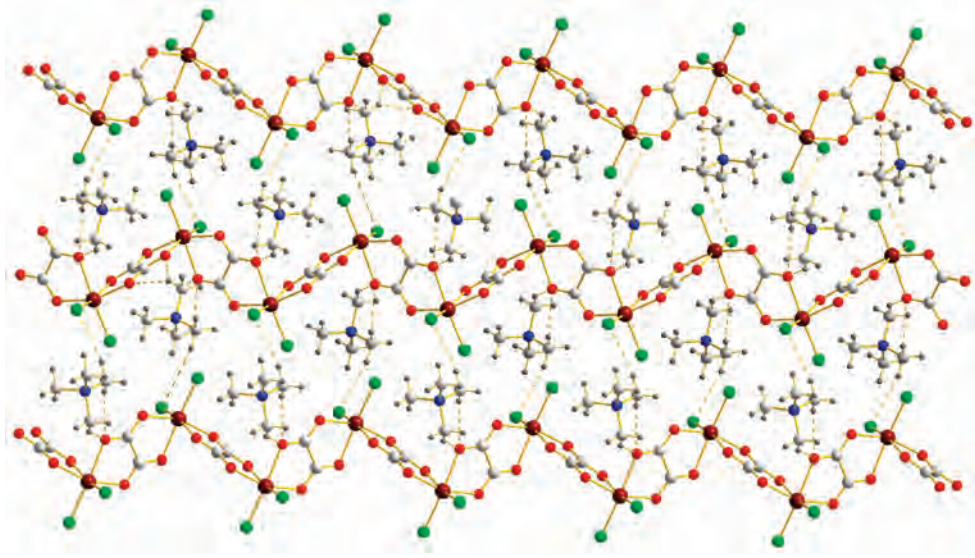

Figure 9. View along the *x* axis showing the supramolecular motif in compound **11b**.

Having in mind the 1D structure of **9**−**11**, we have analyzed their magnetic susceptibility data through Fisher's nearest-neighbor classical Heisenberg coupling model for infinite linear chains[51] by eq 1 [where $u(K) = \coth K - (1/K)$ and $K = 35\ J/4kT$], which was derived from the Hamiltonian (2) with $S_i = S_{i+1} = {}^5/_2$.

$$X_M = 35N\beta^2g^2/12kT[1 + u(K)/1 - u(K)] \qquad (1)$$

$$H = -J\sum_{i=1}^{n} S_i \cdot S_{i+1} - g\beta\sum_{i=1}^{n} = H \cdot S_i \qquad (2)$$

In these expressions, N, g, and β have their usual meanings and J is the intrachain magnetic coupling. A least-squares fit of the susceptibility data leads to the following sets of parameters: $J = -8.4\ cm^{-1}$, $g = 1.99$, and $R = 1.1 \times 10^{-5}$ for **9**, $J = -6.9\ cm^{-1}$, $g = 1.99$, $\rho = 0.3\%$, and $R = 2.1 \times 10^{-5}$ for **10**, and $J = -8.4\ cm^{-1}$, $g = 1.99$, $\rho = 0.5\%$, and $R = 1.5 \times 10^{-5}$ (R is the agreement factor defined as $\sum_i[(\chi_M)_{obs}(i) - (\chi_M)_{calc}(i)]^2/\sum_i[(\chi_M)_{obs}(i)]^2$). ρ is the percentage of an impurity of high-spin iron(III) with the same formula weight as those of **10** and **11**, which accounts for the increase of χ_M in the very low temperature range of Figures S3 (**10**) and S4 (**11**) in the Supporting Information.

The antiferromagnetic coupling in **9**−**11** is in agreement with the previously reported results for other oxalato-bridged dinuclear and 1D iron(III) complexes (values of $-J$ ranging from 6.8 to 8.6 cm^{-1}).[35b,44,49,52–54] The remarkable ability of the oxalate bridge to mediate relatively important antiferromagnetic interactions in homometallic species where the paramagnetic centers are separated by more than 5 Å is well-

(51) Fisher, E. M. *Am. J. Phys.* **1964**, *32*, 343.

(52) (a) Julve, M.; Kahn, O. *Inorg. Chim. Acta* **1983**, *76*, L39. (b) Lloret, F.; Julve, M.; Faus, J.; Solans, X.; Journaux, Y.; Morgenstern-Badarau, I. *Inorg. Chem.* **1990**, *29*, 2232.

(53) Rashid, S.; Turner, S. S.; Day, P.; Light, M. E.; Hursthouse, M. B. *Inorg. Chem.* **2000**, *39*, 2426.

(54) Coronado, E.; Galán-Mascarós, J. R.; Gómez-García, C. J. *J. Chem. Soc., Dalton Trans.* **2000**, 205.

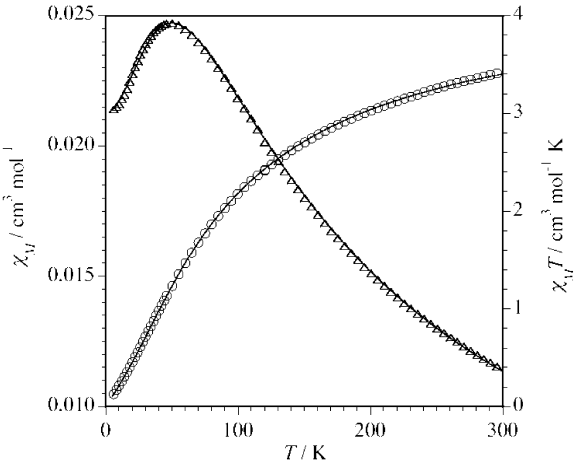

Figure 10. χ_M and $\chi_M T$ versus T plots for compound **9**: (○ and Δ) experimental data; (—) best-fit curve through eq 1.

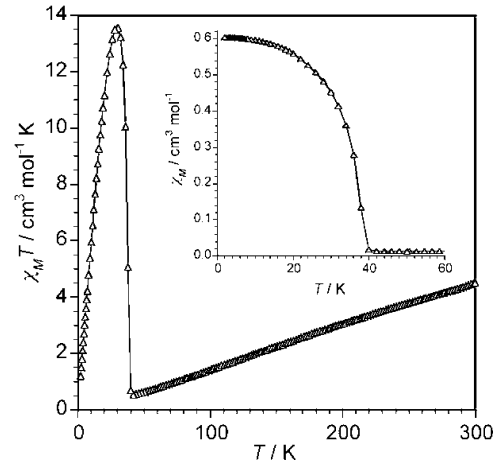

Figure 11. Thermal variation of the $\chi_M T$ product for **4**. The inset shows the low-temperature region of the χ_M versus T plot at $H = 100$ G. The solid lines are guides for the eyes.

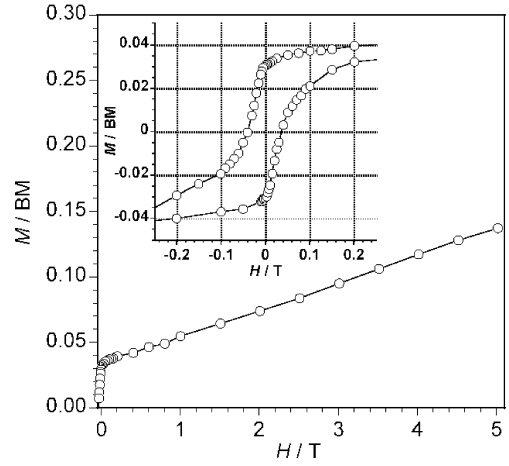

Figure 12. Magnetization versus H plot for **4** at 2.0 K. The inset shows the hysteresis loop at 2.0 K.

known from both experimental and theoretical points of view, in particular in the case of copper(II) compounds,[55] and further comments on this ability seem then unnecessary.

It deserves to be noted that the structure (at room temperature) and the variable-temperature magnetic study of **11**were part of a very recent report where the authors pointed out the occurrence of a very weak spin canting with T_c close to 9 K. We did not observe this feature in our study on **11**.[35] Given the isotropic character of the high-spin iron(III) ion, this phenomenon could only be due to the antisymmetric exchange (see below), but the resulting spin canting would vanish in the case of a centric space group. Because the space group of **11** is $P2_1/c$, a structural change into an acentric space group at temperatures greater than T_c could be at the origin of the spin canting of this compound. This is why we performed the X-ray characterization of the crystal structure of **11** at both room temperature and 9.0 K in order to check the possibility of this structural change. Because the same centric spatial group was observed at both temperatures, we conclude that the spin canting observed by the other authors is most likely due to a small impurity [a highly probable feature because **11** was prepared by them in neutral or slightly basic aqueous solutions where a significant hydrolysis of iron(III) could be involved]. In our case, this impurity could be avoided because the preparation of crystals of **11** was performed in a quite acidic aqueous solution (see the experimental part).

3D Oxalato- and Oxo/Hydroxo-Bridged Iron(III) Compounds. The thermal variation of the $\chi_M T$ product for **4** [χ_M is the magnetic susceptibility per two iron(III) ions] under an external magnetic field of 100 G is shown in Figure 11. At room temperature, $\chi_M T$ is equal to 4.25 cm^3 mol^{-1} K, a value much smaller than that expected for two magnetically isolated spin sextets [8.75 cm^3 mol^{-1} K for $S = {}^5/_2$ with $g =$ 2.0]. Upon cooling, $\chi_M T$ decreases and it attains a minimum at 42 K. Below this temperature, $\chi_M T$ increases abruptly to reach a maximum at 27 K ($\chi_M T = 13.70$ cm^3 mol^{-1} K), and in the very low temperature range, $\chi_M T$ decreases linearly with T and it vanishes. The χ_M versus T plot for **4** exhibits a rapid increase below 40 K (see the inset of Figure 11). These features can be attributed to a spin canting. The magnetization versus H plot at 2.0 K (Figure 12) exhibits a *quasi*-plateau at low magnetic fields (M ca. 0.035 μ_B) and then increases linearly to reach a maximum value of ca. 0.14 μ_B at 5 T. The hysteresis loop of **4** at 2.0 K (see the inset of Figure 12) shows values of the coercive field (H_c) and remnant magnetization (M_r) of 410 G and 0.032 μ_B, respectively. From the saturation value of the magnetization of the canting (ca. 0.04 μ_B) and that expected from two spin $S = {}^5/_2$ (10 μ_B), a value of the canting angle of ca. 0.18° is calculated (see Table 7). Similar behavior was observed for the other oxo/hydroxo and oxalato compounds: **1** (Figures S5 and S6 in the Supporting Information), **2** (Figures S7 and S8 in the Supporting Information), **3** (Figures S9 and S10 in the Supporting Information), **5** (Figures 11 and 12), **6** (Figures S13 and S14 in the Supporting Information), **8** (Figures S15 and S16 in the Supporting Information), and

(55) (a) Alvarez, S.; Julve, M.; Verdaguer, M. *Inorg. Chem.* **1990**, *29*, 4500. (b) Glerup, J.; Goodson, P. A.; Hodgson, D. J.; Michelsen, K. *Inorg. Chem.* **1995**, *34*, 6255. (c) Cano, J.; Alemany, P.; Alvarez, S.; Verdaguer, M.; Ruiz, E. *Chem.—Eur. J.* **1998**, *4*, 476. (d) Castillo, O.; Luque, A.; Román, P.; Lloret, F.; Julve, M. *Inorg. Chem.* **2001**, *40*, 5526. (e) Cangussu, D.; Stumpf, H. O.; Adams, H.; Thomas, J. A.; Lloret, F.; Julve, M. *Inorg. Chim. Acta* **2005**, *358*, 2292.

Table 6. Selected Bond Distances (Å) and Angles (deg) for Compounds **10**, **11**, and **11b**[a]

	X =		
	Me_3NH^+ (**10**)	Me_4N^+ (**11**)	Me_4N^+ (**11b**)
Fe(1)−O(1)	2.129(3)	2.120(5)	2.123(4)
Fe(1)−O(2)	2.037(3)	2.070(5)	2.069(4)
Fe(1)−O(3)	2.150(4)	2.159(5)	2.163(4)
Fe(1)−O(4)	2.042(3)	2.019(5)	2.026(4)
Fe(1)−Cl(1)	2.244(2)	2.267(2)	2.287(2)
Fe(1)−Cl(2)	2.233(2)	2.219(2)	2.229(2)
O(2)−Fe(1)−O(4)	158.4(1)	158.6(2)	158.4(2)
O(2)−Fe(1)−O(1)	78.1(1)	78.8(2)	79.0(2)
O(4)−Fe(1)−O(1)	85.6(1)	87.8(2)	87.8(2)
O(2)−Fe(1)−O(3)	85.1(1)	82.5(2)	82.4(2)
O(4)−Fe(1)−O(3)	78.1(1)	78.7(2)	78.4(2)
O(1)−Fe(1)−O(3)	80.0(1)	79.8(2)	79.5(2)
O(2)−Fe(1)−Cl(2)	98.8(1)	99.2(2)	98.5(1)
O(4)−Fe(1)−Cl(2)	95.3(1)	97.6(1)	98.7(1)
O(1)−Fe(1)−Cl(2)	89.7(1)	90.9(1)	90.7(1)
O(3)−Fe(1)−Cl(2)	168.1(1)	170.0(1)	169.8(1)
O(2)−Fe(1)−Cl(1)	92.9(1)	90.6(1)	91.1(1)
O(4)−Fe(1)−Cl(1)	100.7(1)	99.3(2)	98.4(1)
O(1)−Fe(1)−Cl(1)	167.6(1)	165.8(1)	165.8(1)
O(3)−Fe(1)−Cl(1)	90.8(1)	89.5(1)	89.1(1)
Cl(2)−Fe(1)−Cl(1)	100.21(7)	100.24(8)	100.98(7)

[a] Estimated standard deviations in the last significant digits are given in parentheses.

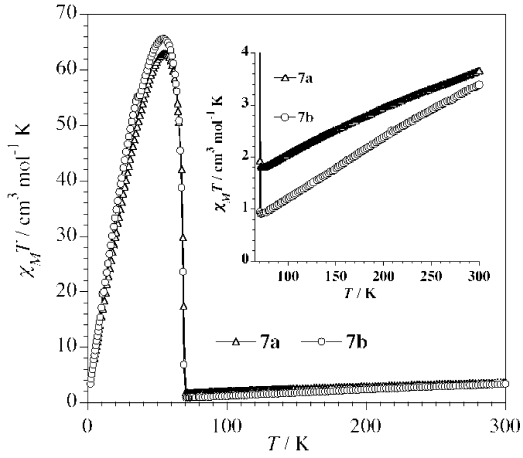

Figure 13. Thermal variation of the $\chi_M T$ product for **7a** and **7b** at H = 100 G. The inset shows the high-temperature region in detail.

7a/7b (Figures 13 and 14), with the most striking magnetic feature in this series being the variation of the T_c value [values of T_c ranging from 26 (**2**) to 70 K (**8**); see Table 7].

The well-known ability of the oxo ($-J$ values covering the 45–240 cm^{-1} range),[32,45] hydroxo ($-J$ values in the 7–17 cm^{-1} range),[45b,56] and oxalato bridges ($-J$ values about 7 cm^{-1})[4,32,35b,44,49,52–54] to mediate strong antiferromagnetic interactions between iron(III) ions accounts for the reduced values of $\chi_M T$ of **1**–**8** in the high-temperature range. The spin-canted phenomenon at low temperatures for these compounds is unambiguously attributed to the antisymmetric exchange, which is compatible with the lack of an inversion center in their structure [the isotropic character of the high-spin iron(III) ruling out the magnetic anisotropy as a source of spin canting].[57] A thorough discussion of this phenomenon

(56) Chen, Z.; Xu, Z.; Zhang, L.; Yan, F.; Lin, Z. *J. Phys. Chem.* **2001**, *105*, 9170.

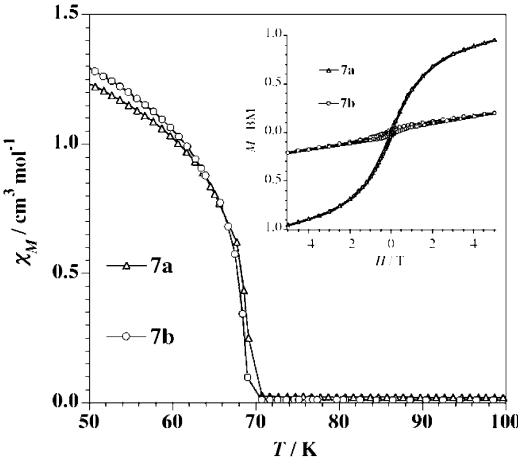

Figure 14. χ_M versus T plot for **7a** and **7b** at H = 100 G. The inset shows the hysteresis loops of **1** and **2** at 2.0 K.

was performed by some of us in a previous report on the related oxalato- and single-oxo-bridged iron(III) compound $\{(NH_4)_2[Fe_2O(ox)_2Cl_2]\cdot 2H_2O\}_n$, which exhibits magnetic ordering at T_c = 40 K,[32] and so we will not add here further comments to that respect.

Let us finish this part with a brief comparison between the magnetic behavior of the related compounds **7a** and **7b**, which is illustrated by Figures 13 and 14. The reduced values of $\chi_M T$ at room temperature, 3.67 (**7a**) and 3.40 cm^3 mol^{-1} K (**7b**) per two iron(III) ions, to be compared with 8.75 cm^3 mol^{-1} K (per two magnetically isolated spin sextets with g = 2.0), reveal the occurrence of a strong antiferromagnetic interaction through the single hydroxo (**7a**) and oxo (**7b**) bridges, with the antiferromagnetic coupling through the oxalato bridge being smaller. The abrupt increase of $\chi_M T$ below 70 K in the two cases is typical of a spin canting, and the field-cooled magnetization reveals the occurrence of magnetic ordering below this temperature (Figure 14). Both are soft magnets as evidenced by the magnetic hysteresis loops of **7a** and **7b** (see inset of Figure 14) with small values of the coercive field and remnant magnetization (Table 7). The relatively high values of T_c for **7a** and **7b** and the observed shift of ca. 30 K of T_c toward higher temperatures in **7b** when compared to the related oxo- and oxalato-bridged 3D iron(III) networks are very appealing. In particular, the comparison between **7b** (T_c = 70 K) and $\{(EtNH_3)_2[Fe_2(ox)Cl_2(\mu\text{-}O)]\cdot H_2O\}_n$ (**6**; T_c = 56 K) is striking. **7b** and **6** crystallize in the orthorhombic system, spatial group *Fdd*2, with the main difference being the occurrence of two different univalent cations in the former (hydronium and ethylammonium cations in **7b** versus two ethylammonium cations in **6**). The cations and the water molecule are located in the pseudohexagonal tunnels defined by oxo- and oxalato-bridged iron(III) networks. This lowering of the symmetry of the cavities seems to be at the origin of the increase of the T_c value in **7b**, suggesting a new strategy for preparing

(57) (a) Ferrer, S.; Lloret, F.; Bertomeu, I.; Alzuet, G.; Borrás, J.; García-Granda, S.; Liu-González, M.; Haasnoot, J. G. *Inorg. Chem.* **2002**, *41*, 5821. (b) Dzyaloshinsky, I. *Phys. Chem. Solids* **1958**, *4*, 241. (c) Moriya, T. *Phys. Rev.* **1960**, *120*, 91.

Table 7. Selected Magnetostructural Data for $\{(NH_4)_2[Fe_2O(ox)_2Cl_2]\cdot 2H_2O\}_n$ and **1**−**8**

X	Fe−O(oxo)/Å	Fe−O(oxo)−Fe/deg	Fe···Fe[a]/Å	T_c/K	H_c[b]/G	M_r[c]/μ_B	α[d]/deg	ref
NH_4^+	1.825(2)	135.9(4)	3.384(2)/5.496(2)	40	4000	0.032	0.18	32
Li^+ (**1**)	1.874(1)	133.6(2)	3.445(19/5.459(1)	51	1100	0.030	0.17	this work
Na^+ (**2**)	1.801(29	136.1(3)	3.341(1)/5.501(1)	26	450	0.012	0.07	this work
K^+ (**3**)	1.804(19	135.4(1)	3.338(1)/5.516(1)	38	1600	0.016	0.09	this work
$MeNH_3^+$ (**4**)	1.873(3)	136.0(5)	3.472(2)/5.462(2)	40	410	0.032	0.18	33
$Me_2NH_2^+$ (**5**)	1.817(5)	136.6(8)	3.377(2)/5.475(3)	52	350	0.026	0.15	33
$EtNH_3^+$ (**6**)	1.809(1)	137.1(2)	3.367(1)/5.496(1)	56	85	0.002	0.02	33
$H_3O^+/EtNH_3^+$ (**7b**)	1.825(3)	136.0(5)	3.384(1)/5.482(1)	70	2500	0.037	0.21	34

X	Fe−OH/Å	Fe−OH−Fe/deg	Fe···Fe[e]/Å	T_c/K	H_c[b]/G	M_r[c]/μ_B	α[d]/deg	ref
$EtNH_3^+$ (**7a**)	1.984(3) 1.882(3)	132.4(2)	3.539(1)/5.525(1)	70	250	0.025	0.14	34
$PrNH_3^+$ (**8**)	1.934(7) 1.926(6)	133.7(4)	3.550(2)/5.457(2)	70	900	0.040	0.23	this work

[a] Iron−iron separation through the oxo/oxalate bridges. [b] Value of the coercive field. [c] Value of the remnant magnetization. [d] Calculated value of the angle of the spin canting (see ref 32). [e] Iron−iron separation across the hydroxo/oxalate bridges.

high T_c iron(III) compounds through the use of different cations to neutralize the charge of the anionic oxo- and oxalato-bridged iron(III) 3D network. Magnetostructural studies on additional examples containing pairs of univalent cations are in route to illustrate and clarify this strategy.

Finally, an inspection of the data listed in Table 7 shows that there is no clear correlation between the shift of T_c and the structural parameters in **1**−**6** and **7b**. However, in this work we clearly demonstrate that the insertion of alkyl groups in the ammonium cation appears as a suitable tool to tune the value of T_c of these 3D compounds. Of course, much remains to be done in order to understand the detailed relation of the canting with the crystal structure as a function of countercation X. Our first attempts using alkaline cations afforded the 3D network with T_c values close to those of the alkylammonium substituted derivatives. Finally, coupled magnetostructural studies on single crystals (X-ray and neutron diffraction experiments) will be performed in the future in order to get a deeper knowledge of the spin canting observed in this family.

Conclusions

A series of oxalate-bridged iron(III) coordination polymers have been reported whose structures and magnetic properties can be tuned. Two different kinds of compounds, 1D and 3D polymers, have been obtained by varying the nature and the shape of the counterion. These results have been useful to point out the influence of the cation on the final structures and its templating effect. The magnetic properties of these compounds have also been extensively studied in order to investigate the role of the cations as guests.

The appropriate conditions for the selective preparation of the 1D or 3D networks were carefully established, on the basis of the templating cation, the crystallization time, and the oxalate-to-cation molar ratio. Remarkably, structural switching from 1D to 3D coordination polymers is essentially driven by the shape and sterical hindrance of the cationic guest in the molecular assembly. 3D networks of oxo- and oxalato-bridged iron(III) ions of the general formula $\{X_2[Fe_2O(ox)_2Cl_2]\cdot pH_2O\}_n$ have been obtained for $X = Li^+$ (**1**), Na^+ (**2**), and K^+ (**3**) ($p = 4$) and $X = MeNH_3^+$ (**4**), $Me_2NH_2^+$ (**5**), and $EtNH_3^+$ (**6**) ($p = 2$). Similar 3D hydroxo/oxalato-bridged iron(III) networks of the formula $\{X[Fe_2(OH)(ox)_2Cl_2]\cdot 2H_2O\}_n$ resulted for $X = EtNH_3^+$ (**7a**) and $PrNH_3^+$ (**8**). Compound **7a** undergoes a solid-to-solid transformation, leading to a new species of the formula $\{(H_3O)(EtNH_3)[Fe_2O(ox)_2Cl_2]\cdot H_2O\}_n$ (**7b**). It is noticeable that only with the $EtNH_3^+$ cation both hydroxo/oxalato (**7a**) and oxo/oxalato (**6**) 3D species were obtained, with this cation delimiting an ideal frontier between the oxo- and hydroxo-bridged compounds. Chainlike compounds of the formula $\{X_2[Fe_2(ox)_2Cl_4]\cdot pH_2O\}_n$ [$X = Me_2NH_2^+$ (**9**, $p = 1$), $Me_3NH_2^+$ (**10**, $p = 2$), and Me_4N^+ (**11**, $p = 0$)] have been obtained for the bulkier alkylammonium cations. The unfeasibility to build the 3D network with these bulkier cations may be due to the purposeful selection of the 3D cavities, with the dimethylammonium cation being a borderline cation in the construction of 3D or 1D compounds.

Magnetic susceptibility measurements show the occurrence of weak ferromagnetic ordering due to spin canting in the 3D networks, with the value of the critical temperature (T_c) varying with the cation in the range 26 K (**2**) to 70 K (**8**). The last three 1D compounds exhibit the typical behavior of antiferromagnetically coupled chains of interacting spin sextets. These results illustrate a strong guest-dependent magnetic behavior (in particular dealing with the T_c value) for the porous materials **1**−**8**, in spite of the fact that no significant structural modifications have been produced in the net by varying the counterions. On the contrary, the slight modification produced in the metal coordination sphere by the single-crystal-to-single-crystal transformation of **7a** into **7b** does not affect the T_c value of the compounds, but it induces significant changes in the values of H_c and M_r.

In conclusion, the present work provides experimental evidence of the key role of the cation guest in dictating the final supramolecular structure and its magnetic properties. In addition, it provides the opportunity to modulate the magnetic properties of these materials and then to improve their performances. Considering the lowering of the symmetry of the cavities in **7b**, which seems to be at the origin of the increase of the value of T_c of ca. 30 K with respect to the isostructural compound **6** [small but significant structural differences concerning the values of the Fe−O(ox) bond length and Fe−O(oxo)−Fe bond angle (see Table 7) cannot

be disregarded], a new strategy to prepare high-T_c iron(III) compounds can be proposed through the use of different cations to neutralize the charge of the anionic oxo/oxalate-bridged iron(III) 3D network.

Acknowledgment. This research was supported by the Italian MIUR, the Spanish MEC (Project CTQU2004-03633), and the EU (Project QueMolNa MRTN-CT-2003-504880).

Supporting Information Available: X-ray crystallographic files in CIF format for **1**−**3**, **8**, **9**, **10**, and **11b**, magnetic plots for **10** (Figure S3), **11** (Figure S4), **1** (Figures S5 and S6), **2** (Figures S7 and S8), **3** (Figures S9 and S10), **5** (Figures S11 and S12), **6** (Figure S13 and S14), and **8** (Figures S15 and 16), and figures of the packing of compound **9** (Figure S1 and S2). This material is available free of charge via the Internet at http://pubs.acs.org.

IC702403H